[AMERICAN JOURNAL OF SCIENCE, VOL. 293, NOVEMBER, 1993, P. 894–938]

MISSING MINERAL ZONES IN CONTACT METAMORPHOSED BASALTS

CRAIG E. MANNING,* STEVEN E. INGEBRITSEN,** and DENNIS K. BIRD***

ABSTRACT. **We describe an extreme example of the kinetic controls on the contact metamorphism of basalts in which a predicted mineral zone is missing. In the metabasalts that host the Skaergaard intrusion in East Greenland, a high-grade pyroxene hornfels (the *pyroxene zone*) is in contact with a low-grade greenschist-facies mineral assemblage (the *actinolite + chlorite zone*). Hornblende-bearing assemblages are absent, and there is no evidence that they ever formed. The boundary between the two mineral zones occurs at 250 m from the contact and records an abrupt change in metamorphic temperature as well as mineral assemblage and texture. Mineral assemblages for the high-grade rocks reflect peak metamorphic temperatures that decreased from ~900°C at the contact to ~800°C at 250 m. Beyond this distance, the greenschist-facies mineral assemblages replacing relict igneous minerals suggest temperatures of 300° to 550°C. Numerical simulations of heat and fluid flow for a model approximating the geometry of the Skaergaard magma-hydrothermal system reproduce the peak temperatures observed within 100 m of the contact only for basalt permeabilities of less than or equal to $\sim 10^{-16}$ m^2. Whole-rock $\delta^{18}O$ values suggest cumulative fluid fluxes that require basalt permeability $\geq 10^{-16}$ m^2. The thermometry and isotopic data thus combine to constrain permeability to have been $\sim 10^{-16}$ m^2. The abrupt change in metamorphic temperatures inferred from the mineral assemblages was not predicted in the simulations, implying that the 250 m boundary was caused by reaction kinetics. If metamorphic reactions had proceeded such that chemical equilibrium was approached closely, the formation of hornblende should have occurred at ~550°C. For a permeability of 10^{-16} m^2, this temperature was overstepped by ~80°C at 250 m when peak temperatures were attained in the simulations. The extent of oxygen isotope alteration suggests transport processes were not rate limiting, and dissolution of the most refractory mineral, clinopyroxene, would have been too rapid to explain the missing mineral zone. Using equations describing temperature oversteps required to achieve observable nucleation rates, we show that the low entropy changes of model metamorphic reactions involving hornblende formation imply that large oversteps of hornblende nucleation reactions are possible and that hornblende nucleation was rate limiting. Missing mineral zones appear to characterize basaltic contact aureoles where the protolith was unaltered, and metamorphism was not progressive.**

INTRODUCTION

Contact metamorphic aureoles preserve a geologic record of large gradients in temperature, strain, and fluid properties near intrusive

* Department of Earth and Space Sciences, University of California, Los Angeles, Los Angeles, California 90024-1567.
** U.S. Geological Survey, 345 Middlefield Road, Menlo Park, California 94025.
*** Department of Geology, Stanford University, Stanford, California 94305.

igneous bodies. Field-based studies of these environments typically reveal changes in mineral assemblages (mineral zones), bounded by isograds, that correlate with distance from intrusive contacts. The distribution and spacing of mineral zones and isograds contain clues about the interplay between the flow of heat and fluid in contact aureoles (Parmentier and Schedl, 1981; Bowers, Kerrick, and Furlong, 1990; Ferry, 1991; Barton and others, 1991). Because rapid changes in temperature in this environment can lead to large deviations from chemical equilibrium, the geometries of mineral zones and isograds may depend strongly on rates of heterogeneous metamorphic reactions (Lasaga, 1989; Kerrick, Lasaga, and Raeburn, 1991; Lasaga and Rye, 1993). Near equilibrium, reactions among the aluminosilicate polymorphs occur at low rates, so kinetic effects on isograds are often discussed for the pelitic bulk compositions in which these minerals are common (Lasaga, 1986). But common disequilibrium textures suggest that kinetic effects are also important in the contact metamorphism of mafic rocks (Tracy and Frost, 1991).

Field, experimental, and theoretical studies on basaltic bulk compositions lead to a petrogenetic grid that predicts changes in equilibrium mineral assemblage with temperature in mafic contact aureoles (Liou, Kuniyoshi, and Ito, 1974; Liou, Maruyama, and Cho, 1985; Turner, 1981; Spear, 1981; Maruyama, Suzuki, and Liou, 1983; Moody, Meyer, and Jenkins, 1983). At low to moderate pressures and temperatures less than $\sim$500°C, the greenschist-facies assemblage of actinolite, chlorite, albite, epidote, quartz, sphene, and magnetite is stable. These minerals give way to an intermediate-temperature assemblage of hornblende, calcic plagioclase, and ilmenite with increasing temperature. At higher temperatures, hornblende-breakdown reactions form clinopyroxene, orthopyroxene, and olivine. Hornblende is absent at the highest temperatures, and mineral assemblages include two pyroxenes, olivine, labradorite, and Fe-Ti oxides with sporadic biotite. Many mafic contact aureoles display a regular progression of these mineral assemblages (Tracy and Frost, 1991). Well-studied examples include Karmutsen, British Columbia (Kuniyoshi and Liou, 1976b), Diamond Hill, New South Wales, Australia (Andrew, 1984; Andrew and O'Neil, 1988), Mt. Tallac and Bear Mountain, California (Loomis, 1966; Snoke, Quick and Bowman, 1981), and Morton Pass, Wyoming (Russ-Nabelek, 1989). In contrast, at least two localities in the North Atlantic Tertiary Province display greenschist-facies mineral assemblages in contact with pyroxene-bearing, hornblende-absent assemblages. Thus, mineral zones recording very high temperatures and low temperatures are juxtaposed, with no evidence that intervening medium-temperature mineral zones ever formed. Missing mineral zones have been documented at Skye, Scotland (Almond, 1964; Ferry, Mutti, and Zuccala, 1987) and at the Skaergaard intrusion, East Greenland (Manning and Bird, 1991, 1993).

In this paper we discuss missing mineral zones in metamorphosed mafic rocks by focusing on the basaltic country rocks of the Skaergaard

intrusion. We combine estimates of metamorphic temperatures and numerical simulations to show that missing mineral zones in the North Atlantic Tertiary Province are kinetic features controlled by low nucleation rates of hornblende.

GEOLOGIC BACKGROUND

The regional geology near the Skaergaard intrusion is shown in figure 1. Early Tertiary rifting in central East Greenland produced a northeast-trending basin in Precambrian basement gneisses. Several hundred meters of Late Cretaceous to Early Paleocene clastic sediments were initially deposited, then voluminous basaltic lavas, breccias, and tuffs rapidly filled the basin (Soper and others, 1976a,b; Nielsen, 1978; Brooks, 1980; Nielsen and others, 1981; Brooks and Nielsen, 1982a,b; Larsen and Watt, 1985; Larsen, Watt, and Watt, 1989). The earliest of the basaltic lithologies, the Vandfaldsalen and Miki Formations, comprise most of the host rocks of the Skaergaard intrusion (fig. 1). The stratigraphic thickness of extrusive material varied widely in the East Greenland Tertiary province, but at the time of emplacement of the Skaergaard magma (~55 Ma; Brooks and Gleadow, 1979; Hirschmann, 1992), the base of the basalts in the area of figure 1 was probably 6 to 7 km below the surface (Brooks and Nielsen, 1982b; Rosing and Lesher, 1992).

Crystallization and cooling of the tholeiitic magma caused the circulation of heated ground water that led to mineralogic and oxygen isotope alteration of the gabbros and country rocks (Wager and Deer, 1939; Wager and Brown, 1967; Myers, 1978; Taylor and Forester, 1979; Norton and Taylor, 1979; Norton, Taylor, and Bird, 1984; Bird and others, 1985; Bird, Rogers, and Manning, 1986; Bird, Manning, and Rose, 1988; Manning and Bird, 1986, 1990, 1991, 1993). In detailed field, petrologic, and geochemical studies east of the intrusion (fig. 2), Manning and Bird (1991, 1993) outlined the metamorphic and structural record of heat and fluid flow during contact metamorphism associated with the Skaergaard intrusion. Five mineral zones were distinguished in this region. Table 1 summarizes key features of these zones. Within 250 m of the contact, the basalts are completely recrystallized to granoblastic-polygonal textures and high-grade mineral assemblages. The *pyroxene zone* is found between 10 and 250 m and consists of Ca-rich and Ca-poor pyroxene, labradorite, and ilmenite. A narrow region within 10 m of the contact, the *olivine zone,* contains these minerals as well as olivine and represents a zone of partial melting during metamorphism (Manning, 1989). In the *actinolite + chlorite zone* (250 m to 2 km), relict igneous minerals are replaced by an upper greenschist facies mineral assemblage of actinolite, chlorite, oligoclase, sphene, quartz, and magnetite with sporadic epidote and K feldspar. Lower grade assemblages of the *prehnite + epidote* and *zeolite zones* are found beyond 2 km from the contact (fig. 1; Manning and Bird, 1993).

Taylor and Forester (1979) showed that heated meteoric water flowed through the basalts during metamorphism. Oxygen isotope ex-

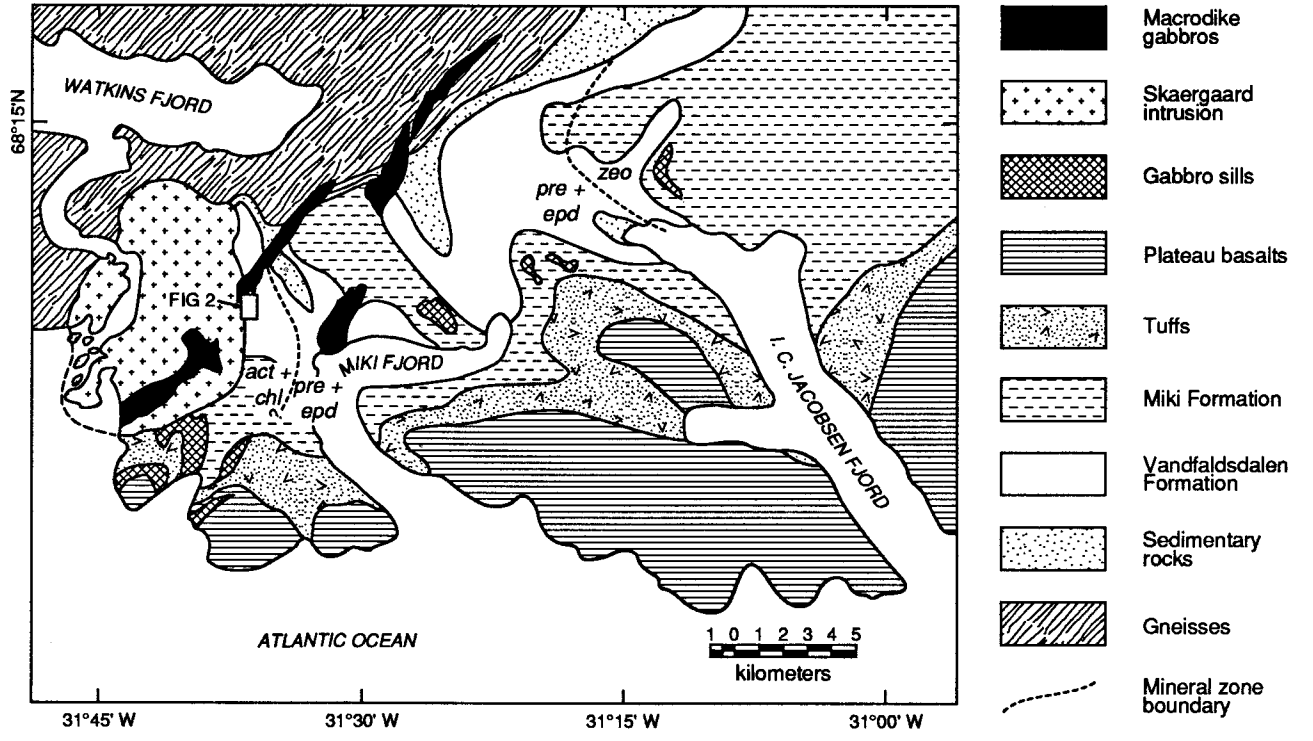

Fig. 1. Geologic map of the region east of the Skaergaard intrusion (after Manning and Bird, 1993). Mineral zone boundaries are shown with heavy dashed lines. The *pyroxene* and *olivine zones* are omitted for clarity. Abbreviations: zeo, *zeolite zone;* pre + epd, *prehnite + epidote zone;* act + chl, *actinolite + chlorite zone.*

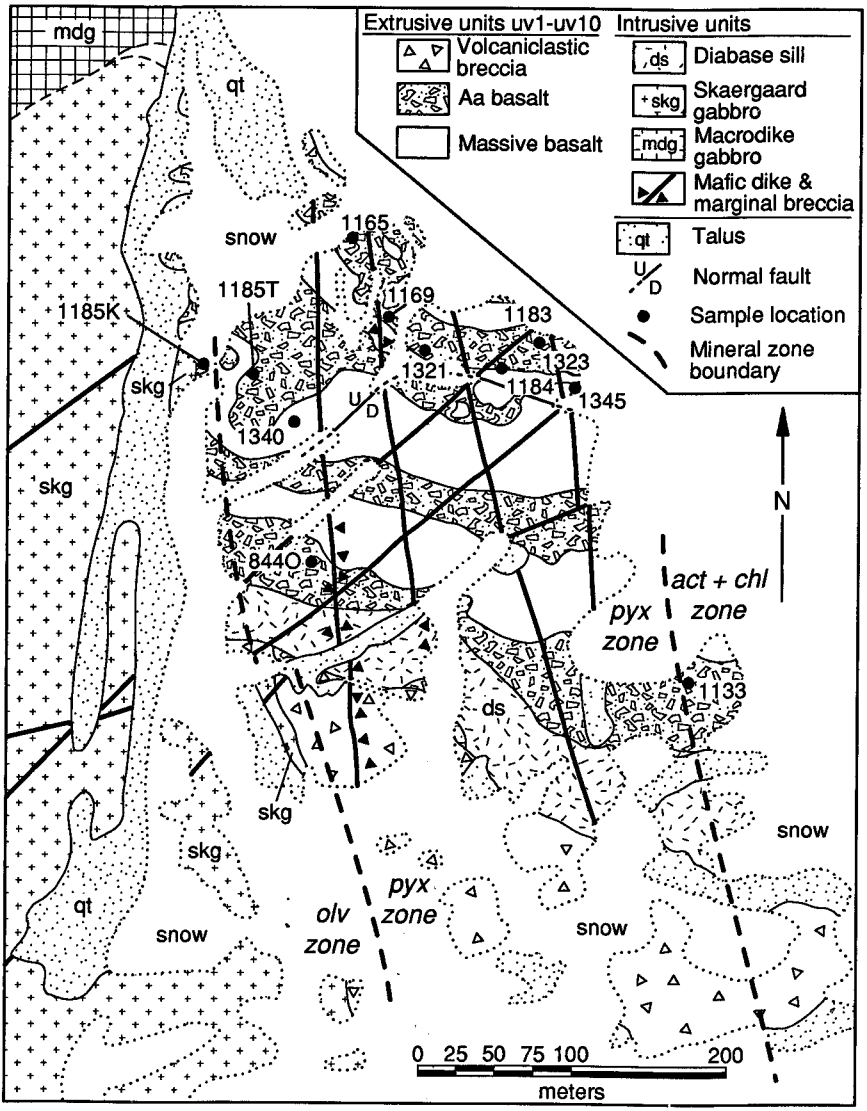

Fig. 2. Geologic map of the study area. See figure 1 for location. Filled circles show locations of samples used for pyroxene thermometry. Mineral zone boundaries are shown with heavy dashed lines. Abbreviations: olv, *olivine zone;* pyx, *pyroxene zone;* act + chl, *actinolite + chlorite zone.*

change reactions led to ^{18}O depletions of up to 4.5 permil (Taylor and Forester, 1979; Manning and Bird, 1993). During prograde heating of the aureole, primary pores such as vesicles and breccia interspace comprised the largest fraction of porosity hosting fluid flow (Manning and

TABLE 1

Summary of metamorphic mineral zones

	Mineral Zone				
	olivine	*pyroxene*	*actinolite + chlorite*	*prehnite + epidote*	*zeolite*
distance from contact	0-10 m	10-250 m	250-2000 m	2 -16 km	>16 km
texture	granoblastic-polygonal hornfels	granoblastic-polygonal hornfels	relict igneous	relict igneous	relict igneous
metamorphic minerals	olv, cpx, opx, plag (lab), bio, ilm	cpx, opx, plag (lab), bio, ilm	act, chl, plag (olig), sph, qtz, mnt, ±epd, ksp	epd, pre, chl, sph, plag (alb), qtz, cal, ±ksp	zeo, pre, chl, sph, plag (alb), qtz, cal, ±ksp
relict igneous minerals	rare cpx phenocrysts	rare cpx phenocrysts	cpx, plag (lab), Fe-Ti oxide	cpx, plag (lab), Fe-Ti oxide	cpx, plag (lab), Fe-Ti oxide

Mineral abbreviations: olv, olivine; cpx, clinopyroxene; opx, orthopyroxene; plag, plagioclase; lab, labradorite; olig, oligoclase; alb, albite; bio, biotite; ilm, ilmenite; act, actinolite; chl, chlorite, sph, sphene; qtz, quartz; mnt, magnetite; epd, epidote; ksp, K feldspar; pre, prehnite; cal, calcite; zeo, zeolite

Bird, 1991). A set of secondary structures, including veins and hydrothermal breccias, also hosted fluid flow during this time. The abundance of these secondary pore types increases as the contact is approached. They are concentrated in units with low average primary porosities, and their morphology changes with distance from the contact. Beyond ~150 m they are horizontal, poorly connected microscopic veins. Between 150 m and the contact, they occur as dominantly vertical, net-like vein swarms. A series of vertical hydrothermal veins formed during retrograde metamorphism. Though these conspicuous structures must have accommodated substantial fluid flow, extents of retrograde alteration are highest in units with high primary porosity, suggesting that primary pores continued to host significant fluid flow during cooling (Manning and Bird, 1993).

Of central importance in this aureole is the juxtaposition of the *actinolite + chlorite zone* with the *pyroxene zone* at 250 m from the contact. The boundary between the zones can not be recognized in the field, but detailed sample traverses reveal that it is abrupt, such that a greenschist-facies assemblage partially replacing igneous minerals gives way within meters to high grade, completely recrystallized pyroxene hornfelses. No aluminous calcic amphiboles occur near the transition (Manning and Bird, 1993), though hornblende-bearing mineral assemblages should be expected from the petrogenetic grid for mafic rocks. Within 250 m from the contact in the *pyroxene zone,* prograde minerals are partially replaced by a retrograde assemblage identical to those found in the *actinolite + chlorite zone.* Hornblende is also absent from the retrograde assemblages.

In addition, Manning and Bird (1993) interpreted whole-rock oxygen isotope compositions as reflecting exchange equilibrium with the meteoric fluids in the *pyroxene zone*, but disequilibrium in the *actinolite + chlorite zone*. The transition from the *pyroxene zone* to the *actinolite + chlorite zone* at 250 m from the contact thus marks a sharp change in mineral assemblage, texture, and oxygen isotope exchange history. Below we show that the peak temperatures of metamorphism inferred from the mineral assemblages also change abruptly at the mineralogic and textural boundary.

TEMPERATURES OF METAMORPHISM

Pyroxene and Olivine Zones

Coexisting metamorphic Ca-rich and Ca-poor pyroxenes occur throughout the *pyroxene* and *olivine zones* (table 1). The compositions of these two phases record temperatures of metamorphic recrystallization through the mutual exchange of Ca, Mg, and Fe (Lindsley, 1983; Davidson, 1985; Davidson and Lindsley, 1985). Anderson, Lindsley, and Davidson (1993) presented internally consistent thermodynamic data and algorithms for computing intensive thermodynamic variables from assemblages of pyroxene, olivine, Fe-Ti oxides, and quartz. Their equations and data allow estimation of temperature of metamorphism using analyzed pyroxene compositions at known pressure.

Compositions of Ca, Mg, and Fe in pyroxenes were determined by electron microprobe and projected into the system CaO-MgO-FeO-SiO_2 for temperature estimation (app. 1). Manning and Bird (1993) gave representative analyses of pyroxenes and coexisting phases. In calculating metamorphic temperature, we used only the compositions of Ca-rich pyroxenes because of the small temperature dependence of the composition of Ca-poor pyroxene (Lindsley, 1983). Also, we assumed that pressure was 2 kb. Uncertainties of 1 to 2 km in depth of burial at the time of Skaergaard emplacement lead to differences in inferred temperature of ≤ 5°C, which is small relative to the range in temperatures derived from different pyroxene grains from the same sample.

Figure 3 shows averages and ranges of inferred temperatures for individual samples in the study area (fig. 2). Calculated metamorphic temperatures decrease with distance from the contact in the *pyroxene* and *olivine zones*. However, the decrease is small: samples near the outer edge of the *pyroxene zone* suggest metamorphic temperatures of ~800°C, only ~100°C less than the mean temperature of sample 1185K, 3 m from the contact. Also, pyroxene compositions are consistent with the textural transition found at the boundary between the *pyroxene* and *actinolite + chlorite zones*. Values of X_{Ca}, defined as $X_{Ca} = n_{Ca}/(n_{Ca} + n_{Fe^{2+}} + n_{Mg})$ where n is the number of moles per six oxygens, decrease from > 0.42 to < 0.40 across this boundary (app. 1; see also Manning and Bird, 1993). Estimated temperatures accordingly increase from ~800°C to >1000°C. The high temperatures suggested by pyroxenes in the *actinolite + chlorite*

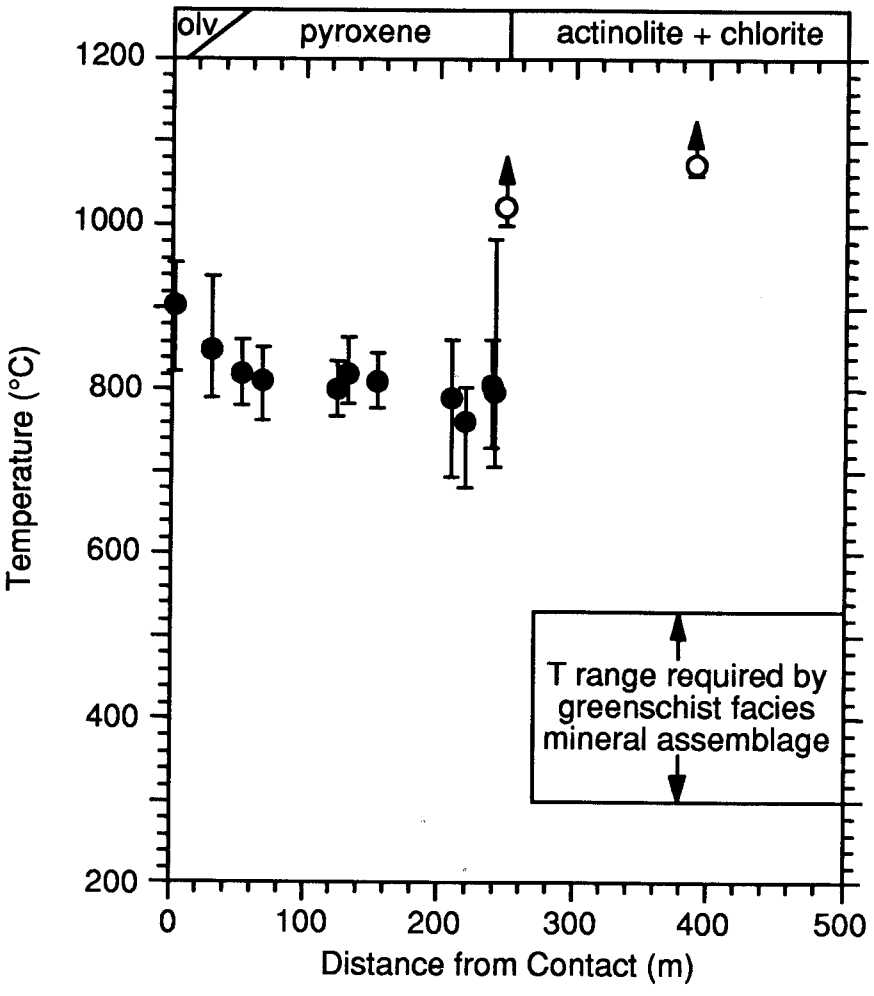

Fig. 3. Temperatures of metamorphism versus distance from the contact in the area of figure 2. Circles are average temperatures calculated from two-pyroxene equilibria, and the bars denote the range in temperatures calculated for each sample (see app. 1). Filled circles represent metamorphic pyroxenes from samples of the *pyroxene* and *olivine zones;* open circles represent igneous pyroxenes from samples of the *actinolite + chlorite zone*. Arrows on pyroxene temperatures in the *actinolite + chlorite zone* signify that these are minimum estimates (see text). The range in metamorphic temperatures implied by the mineral assemblage in the *actinolite + chlorite zone* is shown with the box beyond 250 m from the contact.

zone are minima because Ca-poor pyroxene is absent. They record the original igneous temperatures of crystallization of the pyroxene in the basalts. The wide range in pyroxene compositions at the boundary between the *pyroxene* and *actinolite + chlorite zones* noted by Manning and

Bird (1993) is reflected in the wide range of estimated temperatures shown in figure 3. Manning and Bird (1993) suggested that the variable pyroxene compositions in the outermost *pyroxene zone* are a consequence of partial recrystallization during metamorphism, which implies that in this portion of the aureole, recorded temperatures are not equilibrium values.

Actinolite + Chlorite Zone

Unlike mineral assemblages in the *pyroxene* and *olivine zones*, no individual equilibria allow reliable estimation of temperature for mineral assemblages of the *actinolite + chlorite zone*. However, the range of temperatures over which these minerals could have formed can be inferred. Maximum temperatures of *actinolite + chlorite zone* metamorphism are constrained by the greenschist-amphibolite transition in metabasalts. Liou, Kuniyoshi, and Ito (1974) conducted experiments on low-Al basalts (12-15 wt percent Al_2O_3) and Moody, Meyer, and Jenkins (1983) investigated more aluminous bulk compositions (15-18 wt percent Al_2O_3). The latter authors showed that changes in Al content of amphibole depend in part on bulk rock Al_2O_3 concentration. Since the metabasalts from the study area have 12 to 14 wt percent Al_2O_3 (Manning, 1989), the experiments of Liou, Kuniyoshi, and Ito should be used for comparison. The transition from the greenschist to the amphibolite facies occurs in mafic rocks when mineral assemblages including actinolite, chlorite, and albite react to assemblages including hornblende and labradorite. It occurs over a range of temperatures that depends on pressure and oxygen fugacity for a given bulk composition (Liou, Kuniyoshi, and Ito, 1974; Moody, Meyer, and Jenkins, 1983). The inferred depth of the rocks in figure 2 suggests lithostatic pressures were ~2 kb. Oxygen fugacities during metamorphism were probably at or below the quartz-fayalite-magnetite buffer (Tracy and Frost, 1991). At these conditions, Liou, Kuniyoshi, and Ito (1974) found that chlorite began to decrease in abundance at ~500°C and disappeared from their experimental products at 550°C. Compositions of plagioclase were not reversed, but the experiments suggest that anorthite mole fractions increased from ~0.1 to >0.5 between 500° and 550°C. Tetrahedral Al (^{IV}Al) contents of amphiboles were >0.75 atoms per formula unit (afu) above 550°C and <0.5 afu below 500°C. These results suggest that if assemblages including hornblende (used here for $(Na + K)_A < 0.5$ and $^{IV}Al > 0.75$ afu, Leake, 1978) were to have formed in the contact aureole, temperatures in excess of ~550°C would have been required. Thus, 550°C represents the maximum possible temperature recorded by the mineral assemblage beyond ~250 m from the contact.

Minimum temperatures of metamorphism in the *actinolite + chlorite zone* were ~300°C based on pressure-corrected fluid inclusion homogenization in pore-filling quartz (Manning, 1989). This is consistent with the first appearance of actinolite in active geothermal systems (Bird and others, 1984). These observations indicate that temperatures of forma-

tion of the mineral assemblage found in the *actinolite + chlorite zone* were between 300° and 550°C (fig. 3).

NUMERICAL SIMULATIONS

Textures, mineral assemblages, and estimated metamorphic temperatures all point to an abrupt change in preserved metamorphic conditions at the boundary between the *pyroxene* and *actinolite + chlorite zones*. The progression of mineral assemblages is at odds with the equilibrium petrogenetic grid for metabasalts, in that hornblende-bearing assemblages should have formed between these two mineral zones. To characterize the physical conditions that might have led to the missing mineral zone, we performed numerical simulations of heat and fluid flow for a two-dimensional model Skaergaard magma-hydrothermal system. A full two-dimensional representation of the system allowed us to account for the temporal and spatial changes in the heat and fluid flux vectors, a feature essential to understanding the metamorphism but not possible with simpler, one-dimensional analyses. Norton and Taylor (1979) combined simulations of heat and fluid flow with oxygen isotope data to derive a well-constrained cooling history for this system. We build on this work, accepting many of their assumptions and conclusions, but focusing on the detailed history of the contact aureole.

Computational Methods

We used a modified version of a geothermal simulator, *PT*, described by Bodvarsson (1982). The simulator employs integrated finite difference methods to solve numerical approximations of equations for the conservation of energy and mass, which are respectively

$$\int_V \frac{\partial(\rho_f E_f)}{\partial t}\,dV = \int_A \kappa \nabla T \cdot \mathbf{n} dA - \int_A \rho_f c_f \delta T \mathbf{u} \cdot \mathbf{n} dA + \int_V R_h\,dV \quad (1)$$

and

$$\int_V \frac{\partial(\phi\rho_f)}{\partial t}\,dV = -\int_A \rho_f \mathbf{u} \cdot \mathbf{n} dA + \int_V R_f\,dV. \quad (2)$$

In eqs (1) and (2), V is volume, ρ_f is fluid density, E_f is internal energy of the fluid, t is time, A is area of an interface, κ is thermal conductivity, T is temperature, $\mathbf{n}$ is a unit vector normal to an interface, c_f is the constant-volume heat capacity of the fluid, δT is an interface temperature, ϕ is porosity, and R_h and R_f are heat and fluid source/sink terms. In addition, $\mathbf{u}$ corresponds to the specific discharge (Darcy velocity) calculated from Darcy's law:

$$\mathbf{u} = -\frac{k}{\mu}(\nabla P - \rho_f \mathbf{g}), \quad (3)$$

where k is the permeability, μ is the dynamic viscosity of the fluid, P is the fluid pressure, and $\mathbf{g}$ is the acceleration due to gravity.

The original *PT* code was written to simulate one-phase heat and mass transport in geothermal systems to 400°C assuming constant specific heat of H_2O. We modified *PT* by adding subroutines written by C. W. Mase that compute the properties of H_2O up to 1000°C and 1000 bars using expressions from Keenan and others (1978), Kestin (1978), Meyer and others (1979), and Watson, Basu, and Sengers (1980). Because we assumed a hydrostatic pressure gradient to a depth of 9 km in the model system, fluid pressures remained less than 1000 bars throughout the simulations.

Conceptual Model

Geometry and hydrologic units.—The excellent exposure and detailed mapping of the Skaergaard intrusion provide geometric constraints for use in the simulations. The basalts overlie Precambrian gneisses and were 6 to 7 km thick at the time of Skaergaard emplacement. The thin sequence of sedimentary rocks at the base of the basaltic stratigraphy (fig. 1) was not considered in the simulations. Detailed geologic investigations of the Skaergaard intrusion by Wager and Deer (1939) and Wager and Brown (1967) showed that the intrusion is ~8 km in diameter, elliptical in plan, and 3.5 km in vertical thickness. Norton, Taylor, and Bird (1984) suggested that the body was emplaced rapidly, first as a laccolith, then by faulting the overburden and inflating to its present form. The chamber's margin is approximately vertical and linear for several kilometers to the north and south of the study area (fig. 1; see also Norton, Taylor, and Bird, 1984). A two-dimensional model geometry which ignores shape effects is therefore appropriate for evaluating heat and mass transfer in the area of figure 2.

The geologic observations were used to construct a geometric model of the system (fig. 4). This generalized geologic cross section is made up of four hydrologic units: (1) basalt 1, (2) basalt 2, (3) basement gneisses, and (4) gabbro and basaltic magma. Two basalt units were used to assess the effects of permeability variations on the development of the contact aureole. East of the contact, the boundary between the two units corresponds approximately to the boundary between the *pyroxene* and *actinolite + chlorite zones.*

The thermal and hydraulic properties of the units are summarized in table 2. Gabbro and magma were assumed to have identical thermal and hydraulic properties, with the exception of a higher heat content in the magma due to heat liberation upon crystallization (see below).

Average metabasalt densities increase with increasing metamorphic grade from 2910 kg/m^3 in the *actinolite + chlorite zone,* through 3050 kg/m^3 in the *pyroxene zone,* to 3230 kg/m^3 in the *olivine zone* (Manning, 1989). For simplicity we assumed a constant density of 3000 kg/m^3. This agrees well with values given by Clark (1966) for basaltic rocks. Densities for gneiss and gabbro were also taken from Clark (1966).

Manning and Bird (1991) discussed the evolution of porosity in the metamorphic aureole (fig. 2). The dominant contribution to total poros-

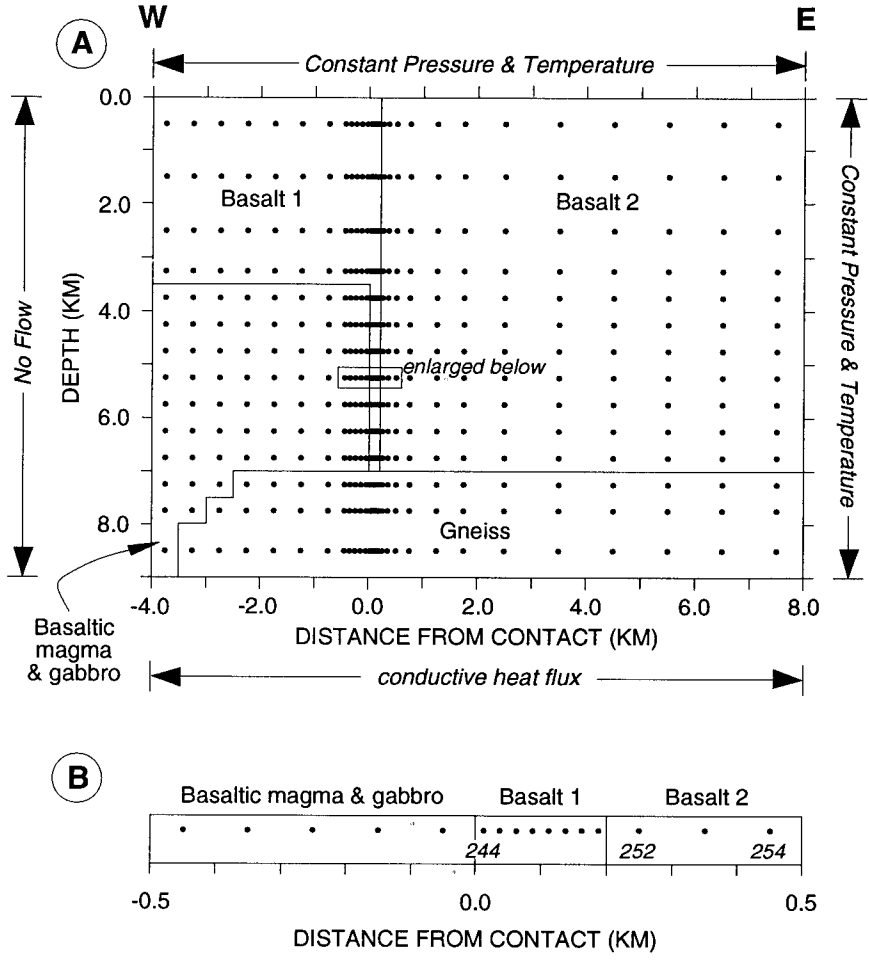

Fig. 4. Conceptual model, node positions, and boundary conditions used in the simulations. The entire simulation region is shown in (A), and the region corresponding to the study area (fig. 2) is shown in (B). The nodes extending out from the contact in (B) are those used in constructing figures 6, 7, and 8. Node 252 in (B) is the node at the interface between the *pyroxene* and *actinolite + chlorite zones*.

ity was primary porosity such as vesicles, vugs, and breccia interspace. Primary porosity ranged from <0.01 to as high as 0.22. We used the mean of 0.05 calculated for all primary porosities in the basalts. Porosities of gabbro and gneiss were set to one order of magnitude lower than those of the basalts, consistent with the absence of macroscopic primary porosity in these units (Manning and Bird, 1991).

Thermal conductivities and heat capacities of mafic rocks show little variation with temperature at high temperatures (Delaney, 1988). We

TABLE 2

Summary of thermal and hydraulic properties of the hydrologic units

Rock Type	Density kg m^{-3}	Porosity	Thermal Conductivity W m^{-1}K^{-1}	Specific Heat J kg^{-1}K^{-1}	Matrix Compressibility Pa^{-1}	Permeability m^2
Basalt 1	3000	0.05	2.0	1000	10^{-10}	variable
Basalt 2	3000	0.05	2.0	1000	10^{-10}	variable
Gneiss	2650	0.005	2.7	1000	10^{-10}	10^{-19}
Gabbro/Magma	3000	0.005	2.0	1000*	10^{-10}	10^{-19}

*Excludes latent heat of crystallization (see text)

therefore used temperature- and pressure-independent values for these parameters from Clark (1966). The thermal effects of metamorphic reactions in the country rocks were ignored, and we assumed no fluid production during metamorphism. Though fluid production is important in the fluid flow histories of many low-permeability mesozonal plutonic environments (Hanson, 1992; Hanson and others, 1993), this simplification is justified by the limited extent of alteration prior to magma emplacement and the comparatively high permeabilities likely for this system (see below). Matrix compressibilities of all units were assigned values sufficiently low to make the matrix effectively incompressible (10^{-10} Pa^{-1}). Both the gabbros and basement gneisses were held at a permeability of 10^{-19} m^2 throughout the simulations. The gabbro permeability adopted here is three orders of magnitude lower than the value inferred by Norton and Taylor (1979). As will be seen below, contact metamorphism occurred in the first 100,000 yr after gabbro emplacement. Since the magma chamber required 130,000 yr to crystallize (Norton and Taylor, 1979), it can be assumed to be essentially impermeable prior to this time.

Node geometry.—Figure 4A shows the geometry of the 527 nodes that comprised the numerical grid. The nodes occupy the centers of rectangles whose mutual interfaces are the planes across which the flow of heat and fluid are calculated in the simulations. Because our interest here is in the contact aureole, where gradients in temperature and fluid pressure were large, we varied node spacings to maximize resolution in this part of the system. Figure 4B shows the portion of the model that corresponds to the stratigraphic level of the area studied (fig. 2). Results from this portion of the grid, that is from 0 to 1000 m east of the contact (fig. 4B, nodes 244-255), were used to compare simulated metamorphic temperatures with those inferred from the mineral assemblages.

Boundary and initial conditions.—Boundary and initial conditions are summarized in figures 4 and 5. The upper boundary of the system was the ground surface, which was assumed to have no topography and to correspond to the water table (fig. 4). The left margin was a no-flow plane of symmetry, and the lower boundary was a no-fluid-flow, fixed-

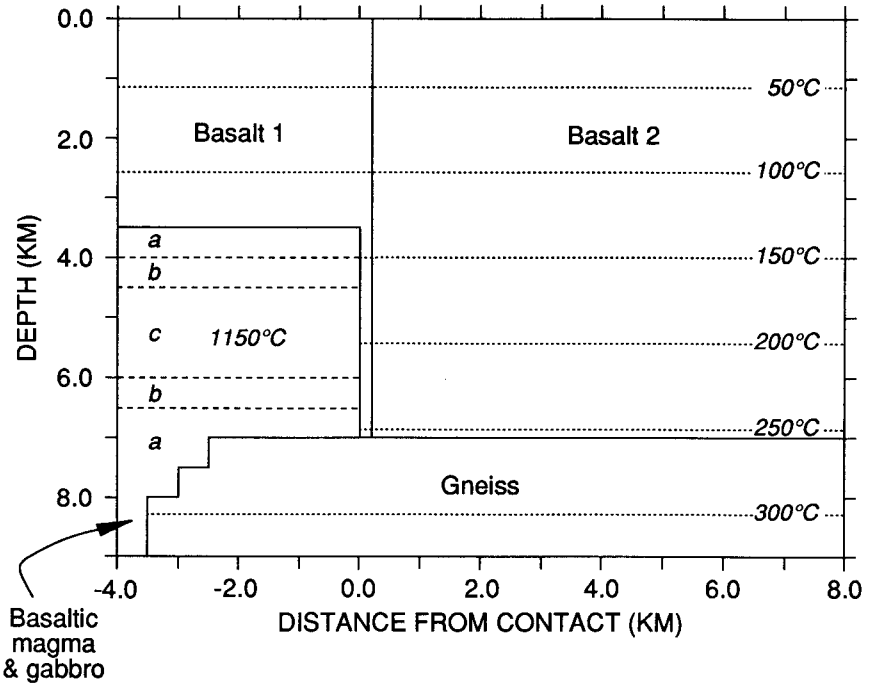

Fig. 5. Initial conditions used in the simulations. Regions in the magma chamber labelled a, b, and c had ΔH_{xln} of 0, 4184, and 8368 J kg^{-1}, respectively. (Compare with fig. 7 of Norton and Taylor, 1979.)

heat-flow boundary. The right margin was held at constant gradients in temperature and pressure corresponding to those selected for the initial conditions of the system. The initial temperature gradient (35°C/km) was constrained by the estimated stratigraphic thickness and the maximum temperatures calculated for fluid inclusion entrapment in secondary quartz near the base of the metabasalt stratigraphy beyond 10 km from the contact (~250°C, Manning, 1989). The steady state geotherm of 35°C/km required conduction of 76 mW/m^2 across the lower boundary, a value consistent with the 50 to 100 mW/m^2 range common in active continental rift zones (Lysak, 1992). This temperature gradient and a corresponding hydrostatic pressure gradient were taken as steady state initial conditions (fig. 5). Magma was assumed to have been instantaneously emplaced into a chamber with the geometry shown in figures 4 and 5. Emplacement temperature of the magma was 1150°C.

Magma Solidification and Latent Heat of Crystallization

An important constraint on the thermal evolution of the magma-hydrothermal system is the geometry of crystallization of the gabbros.

Two geologic observations must be satisfied by the simulations. First, field evidence clearly demonstrates that the Skaergaard intrusion crystallized from the bottom upward and the top downward, forming the sub horizontal modal layering of the layered series and upper border group, respectively (Wager and Deer, 1939; Wager and Brown, 1967; McBirney and Noyes, 1979). This geometry of crystallization implies horizontal crystallization fronts that extended laterally for kilometers. Also, solidification along the sides of the chamber led to the development of the marginal border group, a narrow layer of gabbro that crystallized from the walls inward and is in uncomformable contact with the layered-series gabbros (Wager and Deer, 1939; Hoover, 1989). The width of the marginal border group at the position of the study area ($\sim$250 m) is important because it requires that subsolidus temperatures ($<$1050°C) extended only 250 m into the magma chamber before the solidus was intersected along an upward propagating, horizontal crystallization front in the layered series. In a series of conduction-only experiments, Norton and Taylor (1979) found that the Skaergaard's crystallization geometry could be reproduced with a volume-averaged latent heat of crystallization (ΔH_{xln}) of 4184 J/kg distributed heterogeneously throughout the chamber. This result strongly implies advective redistribution of thermal energy by magma convection in the chamber.

We used the approach of Norton and Taylor (1979): (1) to produce magma/gabbro isotherms that paralleled the chamber's top and bottom and migrated vertically with time, and (2) to keep $T > 1050$°C at >250 m lateral distance into the chamber until the layered series crystallized. In all simulations we maintained an average ΔH_{xln} of 4184 J/kg for the intrusion as a whole (Clark, 1966; Norton and Taylor, 1979). The latent heat of crystallization was liberated uniformly over an assumed crystallization interval of 100°C (1150°-1050°C). The distribution of ΔH_{xln} that reproduced the required crystallization geometry is shown in figure 5 and is similar to that used by Norton and Taylor (1979, see their fig. 7).

The study area is adjacent to a portion of the intrusion with elevated ΔH_{xln}, and its thermal history should reflect the greater quantity of thermal energy at this level of the system. Figure 6 compares the peak temperature profile predicted assuming homogeneous ΔH_{xln} with that computed for the heterogeneous ΔH_{xln} configuration shown in figure 5 for the portion of the model corresponding to the study area (fig. 4B). The heterogeneous ΔH_{xln} distribution that best reproduces the crystallization geometry also agrees well with inferred metamorphic temperatures in the *pyroxene* and *olivine zones,* particularly within 100 m of the contact. If ΔH_{xln} were not advectively redistributed by magma convection, simulated peak temperatures would have been at least 100°C less than those inferred from the mineral assemblages near the contact. Because the limiting case of pure conduction leads to the maximum predicted temperatures in the *pyroxene* and *olivine zones* (see below), we suggest that the metamorphic temperatures in the inner portion of the aureole lend further support to the conclusion that magma convection

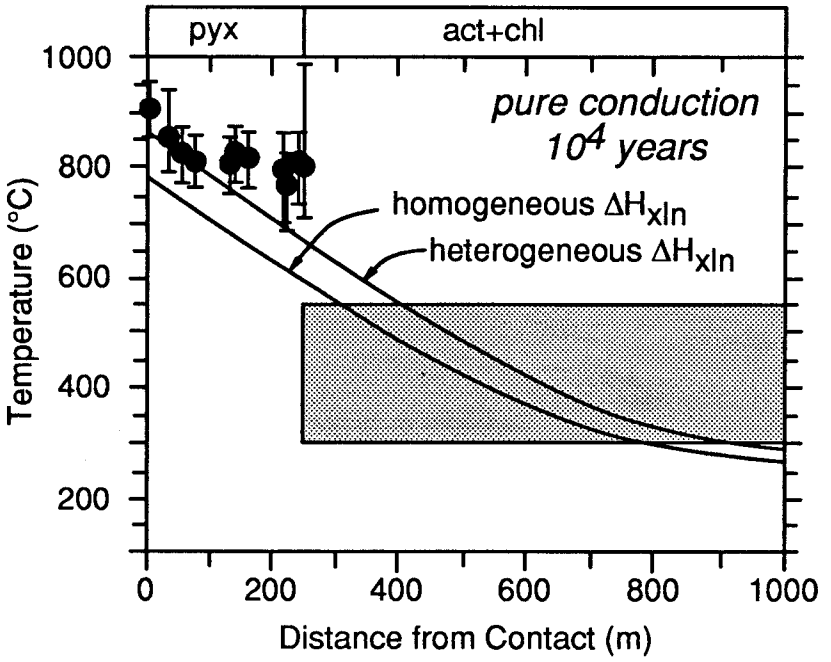

Fig. 6. Comparison of the simulated 10,000 yr temperature profile for a homogeneous ΔH_{xln} with that for the distribution of ΔH_{xln} shown in figure 5. In both cases, maximum temperatures in the *pyroxene zone* were attained at this time. Inferred metamorphic temperatures are taken from figure 3 (see text).

transported substantial quantities of thermal energy in the Skaergaard intrusion.

Simulations with Homogeneous Permeabilities

Permeability is the most important parameter governing heat and fluid transport through the aureole. To examine variations in the advective redistribution of heat by H_2O, we first performed a series of simulations in which basalt permeabilities were time- and space-invariant. Manning and Bird (1991, 1993) discussed the spatial and temporal variations in the pore network. This work showed that the largest fraction of porosity was primary. Also, their oxygen isotopic data suggested that lithologically controlled variations in fluid flux, and thus permeability, were probably not greater than about 10 percent. Averaging system properties over volume on the scale adopted here is therefore appropriate, given the scale of the numerical grid (McKibbon and Tyvand, 1982; Furlong, Hanson, and Bowers, 1991).

Figure 7 shows simulated temperatures for the portion of the aureole shown in figure 4B, using four different homogeneous permeabili-

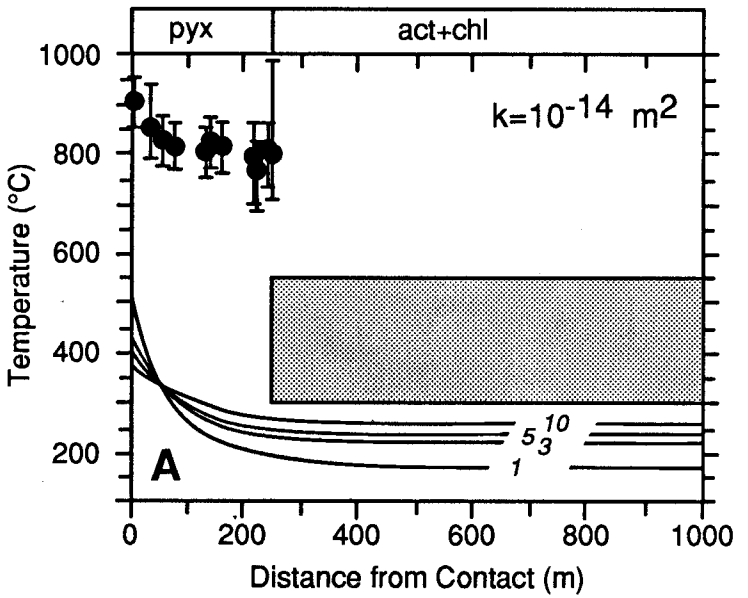

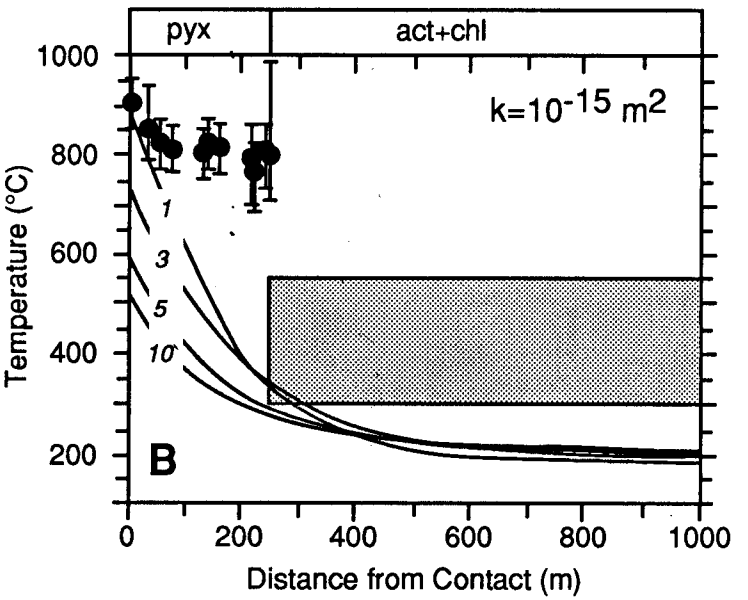

Fig. 7. Simulated temperatures versus distance from the contact at different times for four different homogeneous permeabilities: (A) 10^{-14} m^2, (B) 10^{-15} m^2, (C) 10^{-16} m^2, and (D) conductive (10^{-32} m^2). Labels on curves are in 10^3 yr. The circles and the open box represent the temperatures estimated from the mineral assemblages (fig. 3). The *olivine zone* is omitted for clarity.

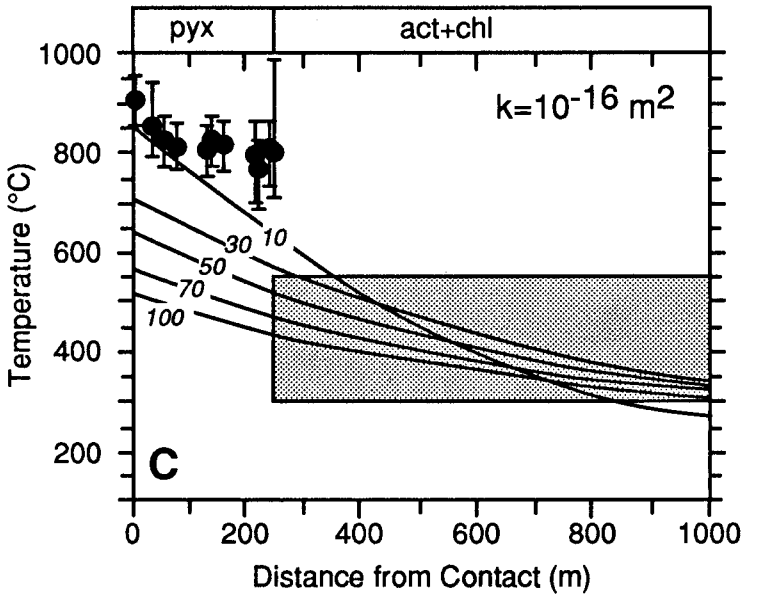
pyx
act+chl
k=10-16 m2
10
30
50
70
100
C
Temperature (°C)
Distance from Contact (m)
1000
800
600
400
200
0
200
400
600
800
1000

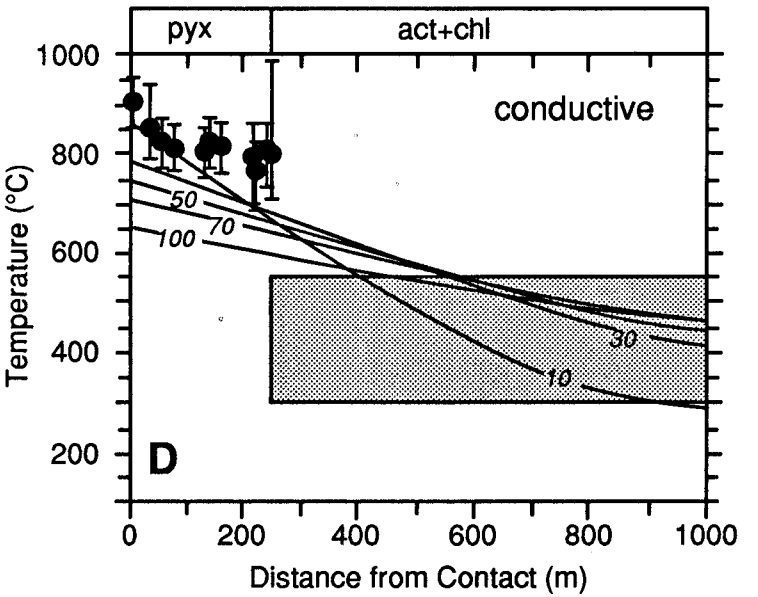
pyx
act+chl
conductive
50
70
100
30
10
D
Temperature (°C)
Distance from Contact (m)
1000
800
600
400
200
0
200
400
600
800
1000

ties. For the high permeability cases (fig. 7A and B), only the early simulation times are shown. The simulations predict that if permeability of the basalts was 10^{-14} m^2, the contact temperature would have been only ~500°C and would have been attained at ≤1000 yr after emplacement. Temperatures in the *pyroxene* and *actinolite + chlorite zones* would have been <300°C, also substantially below the inferred metamorphic temperatures. For basalt permeabilities of 10^{-15} m^2, the maximum temperatures were again attained in the first 1000 yr after emplacement (fig. 7B). The peak contact temperature approached 900°C, but temperatures were <400°C at 200 m for the duration of the simulation. Our estimates of metamorphic temperature recorded in the inner *pyroxene zone* indicate a peak temperature gradient that was less steep. In addition, minimum metamorphic temperatures inferred for the *actinolite + chlorite zone* are greater than those predicted by the simulation for a basalt permeability of 10^{-15} m^2.

Decreasing basalt permeability from 10^{-15} m^2 to 10^{-16} m^2 caused a dramatic change in the simulated cooling history of the aureole (fig. 7B and C). The sharp difference between these models resulted from the change from a hydrothermal system dominated by advective heat transport ($k = 10^{-15}$ m^2) to one dominated by conductive heat transport ($k = 10^{-16}$ m^2). These changes have been discussed in previous analyses of magma-hydrothermal systems (Cathles, 1977; Norton and Knight, 1977; Norton and Cathles, 1979; Parmentier and Schedl, 1981). When basalt permeabilities were 10^{-16} m^2, temperatures within 400 m of the contact increased to maxima in the first 10,000 yr after emplacement and then decreased slowly for the remainder of the simulation. The simulated peak temperatures were within the range of inferred metamorphic temperatures <100 m from the contact in the *pyroxene zone,* but between 100 and 250 m, maximum temperatures were as much as ~150°C below average inferred peak metamorphic temperatures. In the *actinolite + chlorite zone,* temperatures exceeded those recorded by the mineral assemblage between 250 and 350 m from the contact until ~30,000 yr after emplacement but remained within 300° to 550°C elsewhere for the duration of the simulation.

Conductive cooling resulted in peak temperatures in the *pyroxene zone* in 10,000 yr that were ~25°C greater than for the simulation in which $k = 10^{-16}$ m^2 (fig. 7C and D). As with the simulation results shown in figure 7C, there is broad agreement between predicted and inferred temperatures in the inner *pyroxene zone,* though predicted peak temperatures are as much as 100°C below inferred metamorphic temperatures between 200 and 250 m. Simulated temperatures were greater than the temperatures recorded in the inner portion of the *actinolite + chlorite zone* (between 250 and 500 m) for >100,000 yr (fig. 7D).

Simulations with Heterogeneous Permeabilities

Though lithologically controlled permeability variations were probably sufficiently small that they could be ignored in the simulations;

larger scale variations in secondary permeability may have played an important role in the thermal evolution of the aureole. For example, faulting or more extensive fracturing could have led to greater vertical permeability above the intrusion. Also, Manning and Bird (1991) showed that, during prograde metamorphism, pore geometry varied systematically as a function of distance from the contact along the sides of the intrusion. Pore connectivity beyond ~150 m was sub-horizontal, whereas pores became increasingly well-connected vertically within ~150 m. To evaluate the possibility that permeability anisotropy might have contributed to the large change in recorded temperature between the *actinolite + chlorite* and *pyroxene zones*, we performed two additional simulations for each case described above. In the first, we decreased vertical permeability (k_v) beyond 250 m (basalt 2, fig. 4) by a factor of 10 relative to the horizontal permeability (k_h). In the second, we used the same conditions but also increased vertical permeability in the *pyroxene zone* and above the intrusion (basalt 1, fig. 4) by a factor of 10. None of these simulations produced large changes in maximum temperatures in any of the cases, nor did they yield a steep gradient in temperature near the boundary between the *pyroxene* and *actinolite + chlorite zones*. However, they did generate subtle variations in the change in temperature with time. Selected examples of these simulations are shown in figure 8, A and B. Figure 8A shows results of a simulation with predominantly horizontal fluid flow in the outer portion of the system. Changes in temperature with time were virtually identical to those in the conductive simulation (figs. 7D and 8A). Figure 8B shows results of a simulation approximating the possible enhanced vertical connectivity of the pore network near the contact noted by Manning and Bird (1991). Peak temperatures in the *pyroxene zone* were attained in 10,000 yr, and the peak temperature gradient is similar to that shown in figures 7C, D, and 8A.

At any given time in the system's history, temperatures decreased with distance from the contact. Because metamorphic reaction rates depend exponentially on temperature (Fisher, 1978; Walther and Wood, 1984), the high-temperature portions of the aureole near the intrusion may have experienced more rapid pore-filling reactions than lower temperature portions of the aureole. This could have led to a temperature dependent variation in permeability in the aureole. We investigated this scenario by assigning a permeability of 10^{-16} m^2 to the basalts of the *pyroxene zone* along the pluton's margin and a value of 10^{-15} m^2 to all basalts beyond 250 m and above the intrusion. Results of this simulation are given in figure 8C, which shows that peak temperatures were attained in 3000 yr. Temperatures decreased rapidly after peak conditions were attained, and temperatures beyond 400 m from the intrusion were never greater than 300°C.

Simulated versus Inferred Temperatures and Fluid Fluxes

Two types of data can be used to evaluate the degree to which the different permeabilities afford reasonable approximations of the aureole

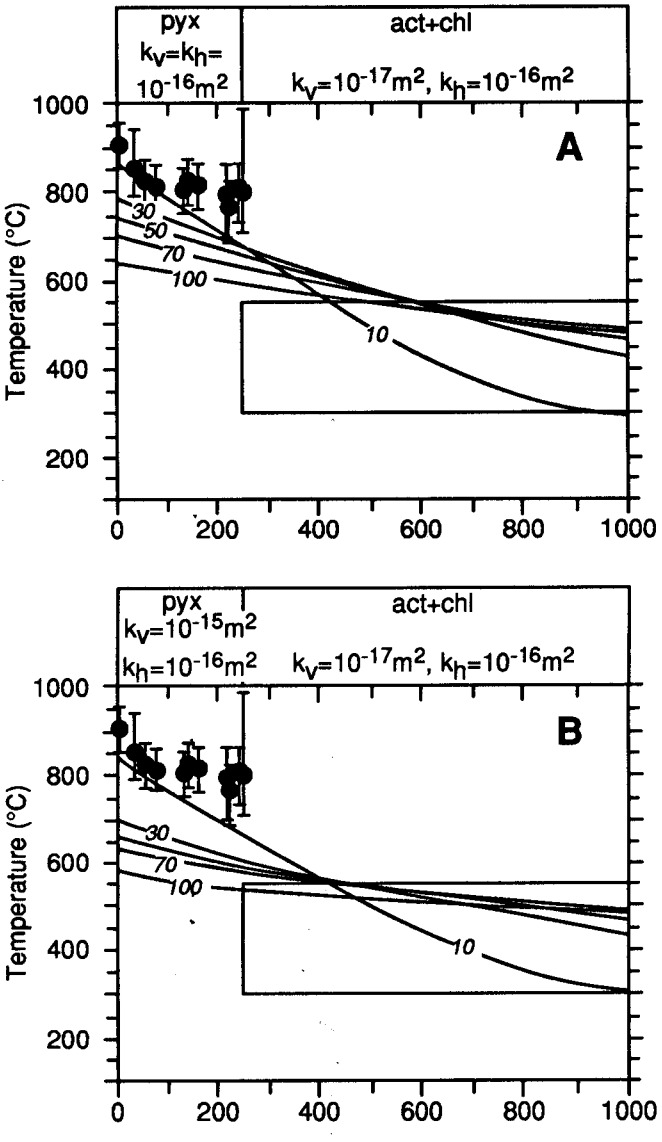

Fig. 8(A), (B), and (C) Simulated temperatures versus distance from the contact at different times for the three heterogeneous permeability structures identified above each plot. The circles and the open box represent the temperatures estimated from the mineral assemblages (fig. 3). The *olivine zone* is omitted for clarity.

for the initial and boundary conditions employed. First, the inferred metamorphic temperatures can be compared with the simulated peak temperatures. We placed particular emphasis on the high-temperature portion of the *pyroxene zone* within 100 m of the contact, where clinopyrox-

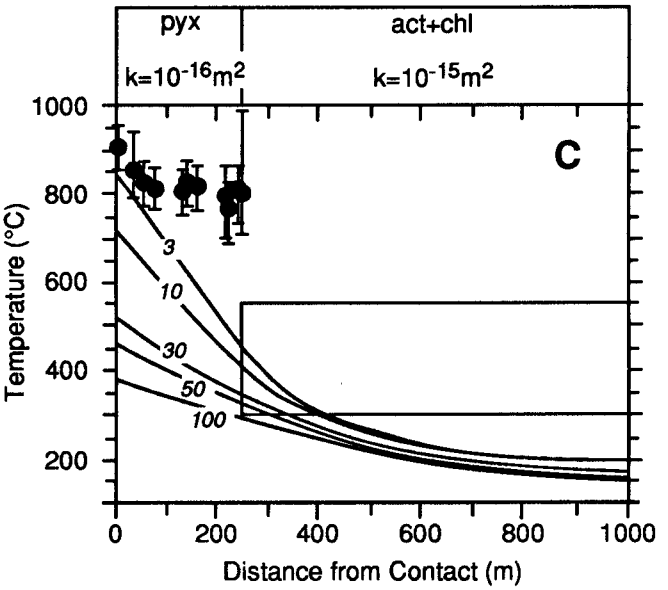

ene compositions most likely reflect equilibrium. Second, cumulative fluid fluxes from the simulations may be compared with those calculated by Manning and Bird (1993) from oxygen isotope ratios.

Temperatures.—Our simulations with homogeneous permeabilities showed that model peak temperatures were in the range of those inferred from clinopyroxene compositions within 100 m of the contact only when permeability was less than $\sim 10^{-16}$ m^2 (fig. 7). Temperatures there increased to maxima within 10,000 yr after emplacement and showed a variation with distance similar to that suggested by the thermometry. In simulations with $k_v \neq k_h$, only those with $k_h \leq 10^{-16}$ m^2 satisfied the same criteria for the inner aureole (fig. 8A and B). When permeability in the *pyroxene zone* was 10^{-16} m^2 but 10^{-15} m^2 elsewhere (fig. 8C), the predicted gradient in peak temperatures was steeper, such that the difference between inferred and simulated peak temperatures at 70 m was $\sim$90°C.

In the outer portion of the *pyroxene zone* (100-250 m), simulated peak temperatures when $k \leq 10^{-16}$ m^2 decreased more strongly than the estimated metamorphic temperatures with increasing distance from the contact. For conductive cooling, the difference between inferred peak temperatures and those predicted is $\sim$100°C at 250 m (fig. 7D). The difference is somewhat greater ($\sim$150°C) for the maximum homogeneous permeability at which the temperatures of the inner *pyroxene zone* were reproduced (10^{-16} m^2, fig 7C). Simulations with heterogeneous permeability display deviations of similar (fig. 8A and B) to much greater magnitudes ($\sim$300°C, fig. 8C). Though uncertainties in estimated meta-

morphic temperatures may be larger than the ranges suggested in figure 3, the contrasting gradients in simulated and inferred peak temperatures point to a different cause for the deviations. One possible explanation is that the metamorphic temperatures are at the lower limits of the experiments upon which Anderson, Lindsley, and Davidson (1992) based their thermodynamic models. This may lead to systematic errors in the temperatures derived from the pyroxene compositions. Alternatively, though all rocks from this interval display the granoblastic-polygonal textures typically assumed to reflect chemical equilibrium, the lower peak temperatures and rapid heating may nevertheless have prevented heterogeneous exchange reactions from proceeding to completion. This is consistent with the wider range in pyroxene compositions and temperatures observed in the outermost *pyroxene zone* (fig. 3; Manning and Bird, 1993). In light of these possibilities, the differences between the inferred and predicted peak temperatures of as much as 150°C between 100 and 250 m are probably not significant. But greater differences suggest an unreasonable permeability. For example, the predicted temperature at 250 m in figure 8C is 300°C less than that inferred. Because temperatures between 200 and 250 m never exceeded those of the *actinolite + chlorite zone* in this simulation, it is unlikely that this model permeability distribution approximates that of the aureole.

The 300° to 550°C temperatures required by the *actinolite + chlorite zone* assemblage were not achieved when homogeneous permeabilities of $\geq 10^{-15}$ m^2 were adopted for all or part of the model (figs. 7A, B, and 8C). When k or $k_h \leq 10^{-16}$ m^2, simulated temperatures beyond 350 to 600 m from the contact fall within the range required by *actinolite + chlorite zone* minerals (figs. 7C and D, 8A and B). Closer to the contact, however, these models predicted temperatures that exceeded the range recorded by the *actinolite + chlorite zone* for at least part of the thermal event. The magnitude and duration of these "oversteps" varied widely. For the conductive case, predicted temperatures were >550°C for >100,000 yr between 250 and 600 m (fig. 7D). The same result was obtained for the case in which $k_v = 10^{-17}$ m^2 in the *actinolite + chlorite zone* (fig. 8A). For the permeability distribution shown in figure 8B, the maximum temperature of 550°C recorded by the minerals of the *actinolite + chlorite zone* was exceeded for ~80,000 yr. In contrast, for homogeneous permeabilities of 10^{-16} m^2, temperature exceeded 550°C between 250 and 350 m for only ~30,000 yr.

Fluid fluxes.—The time- and volume-averaged permeability structure of the basalts can also be constrained by comparing simulated fluid fluxes with those inferred from whole-rock oxygen isotope ratios. Figure 9 shows simulated cumulative, or time-integrated, fluid fluxes for the rock volume centered on node 252 at 250 m from the contact (fig. 4B) as a function of homogeneous basalt permeability. This node represents the boundary between the *pyroxene* and *actinolite + chlorite zones,* so it allows comparison of the simulated fluid flux into the *pyroxene zone* with that inferred from $^{18}O/^{16}O$ patterns in the *pyroxene zone* (Manning and Bird,

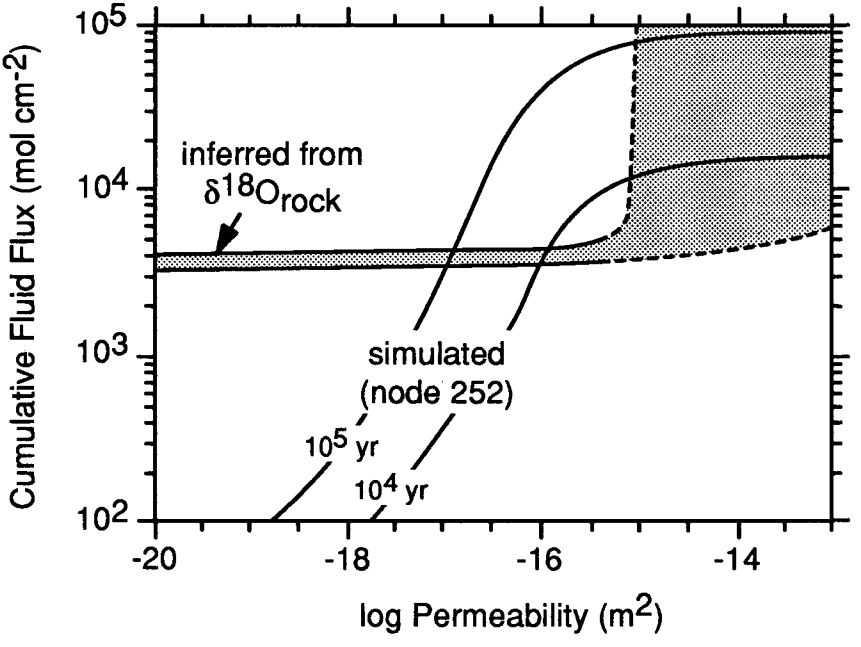

Fig. 9. Comparison of the variation in simulated cumulative fluid flux as a function of permeability with the range inferred from whole-rock oxygen isotope data of Manning and Bird (1993). Simulated cumulative fluxes are from node 252 in the model grid (fig. 4B), which represents the boundary between the *pyroxene* and *actinolite + chlorite zones*. Cumulative fluxes after 10,000 and 100,000 yr are shown with the solid curves. The shaded region represents the range in isotopic fluxes calculated for *pyroxene zone* rocks (see text).

1993). The two curves in figure 9 show cumulative fluxes after 10,000 and 100,000 yr in the simulations. Values increase sharply with increasing permeability to $\sim 5 \times 10^{-16}$ m^2 and then remain unchanged to higher permeabilities.

The time-integrated flux required to generate whole-rock $\delta^{18}O$ compositions can be inferred from one-dimensional equations for stable isotope transport (Bickle and McKenzie, 1987; Baumgartner and Rumble, 1988; Norton, 1988; Blattner and Lassey, 1989; Dipple and Ferry, 1992). Manning and Bird (1993) employed the model of Dipple and Ferry (1992) to estimate time-integrated fluid fluxes in the *pyroxene zone*, the only portion of the aureole in which isotopic equilibrium can be assumed. These calculations assume a time-invariant change in temperature with distance along the flow path, typically the peak metamorphic gradient (Dipple and Ferry, 1992). Using the temperature gradients at 10,000 and 60,000 yr for homogeneous permeabilities of 10^{-16} m^2 (fig. 7C), Manning and Bird (1993) showed that the same cumulative fluxes are obtained by assuming that all isotopic exchange occurred at peak temperatures as by assuming that part of the exchange took place during retrograde alter-

ation. However, the lack of correlation between inferred cumulative fluxes and extents of retrograde alteration in their study strongly implies that isotopic exchange occurred during complete recrystallization of the *pyroxene zone* at peak temperatures. Manning and Bird (1993) used the 10,000 yr temperature gradient for $k = 10^{-16}$ m^2 to demonstrate that 3.6 to 4.0 $\times$ 10^3 mol cm^{-2} of fluid flow is required to explain the ^{18}O depletions in the *pyroxene zone* (fig. 9). Since inferred cumulative flux depends on the temperature gradient and the temperature gradient depends on permeability (figs. 7 and 8), we adopted their input parameters to calculate cumulative fluxes for the peak temperature gradients predicted by different model permeabilities. We used the temperature gradients at the time when peak temperatures were reached within 100 m of the contact for each simulation. The shaded region in figure 9 shows the range in values obtained. Below $k = 5 \times 10^{-16}$ m^2, where simulated peak temperatures are similar because heat transfer was dominantly conductive (fig. 7), cumulative fluid fluxes required to explain the ^{18}O depletions in the *pyroxene zone* are 3 to 4 $\times$ 10^3 mol cm^{-2} and independent of permeability. Predicted peak temperatures at higher permeabilities are so low that some samples permit infinite cumulative fluxes, so the shaded region in figure 9 expands accordingly above $k = 5 \times 10^{-16}$ m^2.

Magnitudes of fluid flow inferred from oxygen isotope data are minimum values since much of the flowing fluid may not exchange oxygen with the rock during metamorphism (Taylor, 1977). Realistic simulation conditions should therefore lead to time-integrated fluxes greater than or equal to those calculated from the $\delta^{18}O$ data. Figure 9 shows that for the most plausible scenario in which all isotopic exchange occurred at peak temperatures, model cumulative fluxes equal or exceed those calculated from the $\delta^{18}O$ data only for homogeneous permeabilities $\geq 10^{-16}$ m^2. If some exchange was retrograde, occurring at any time up to 100,000 yr after emplacement, homogeneous permeabilities as low as $\sim 10^{-17}$ m^2 lead to cumulative fluxes that exceed those inferred from the isotopic data. Simulations with heterogeneous permeabilities summarized in figure 8A and B had cumulative fluxes of 4 $\times$ 10^2 mol cm^{-2} at 10,000 yr after emplacement at node 252; the inferred values 3.6 to 4.0 $\times$ 10^3 mol cm^{-2} require retrograde isotopic exchange.

Summary of simulation results.—Homogeneous permeabilities of $\geq 10^{-15}$ m^2 in all or part of the models resulted in temperatures too low to be consistent with the mineral assemblages in most of the *actinolite + chlorite* and *pyroxene zones* and are therefore unlikely values for the aureole. When homogeneous permeabilities were $\leq 10^{-16}$ m^2, peak temperatures in the *pyroxene zone* and their variation with distance were similar to those inferred. Also, temperatures beyond 500 m remained in the range estimated from mineral assemblages throughout the simulations. Assuming all oxygen isotope exchange in the *pyroxene zone* occurred during prograde metamorphism, the minimal homogeneous permeability in the simulations that can account for the isotopic compositions is $\sim 10^{-16}$ m^2; homogeneous permeabilities of $> 10^{-17}$ m^2 can account for the whole

rock isotopic compositions if some exchange was retrograde. These observations suggest that time- and volume-averaged homogeneous permeability of $\sim 10^{-16}$ m^2 affords the most reasonable match with the geologic observations; a somewhat wider range of between 10^{-17} and 10^{-16} m^2 would be consistent only if significant retrograde isotopic alteration is allowed, a scenario we view as unlikely. Our simulations with heterogeneous permeabilities do not yield significant temperature differences from the homogeneous cases. This suggests that the combined sensitivities of the simulations and thermometry are not sufficient to distinguish between models with homogeneous and heterogeneous permeabilities. However, the low cumulative fluxes at 10,000 yr in the simulations argue against these more complex permeability structures.

Norton and Taylor (1979) adopted a basalt permeability of 10^{-15} m^2 in their detailed simulations of the Skaergaard magma-hydrothermal system. Their work focused on using oxygen isotope ratios of plagioclase to infer permeabilities of the gabbros, and basalt permeability was not constrained. A decrease in time- and volume-averaged permeability from 10^{-15} m^2 to 10^{-16} m^2 significantly alters the predicted temperature and fluid flow history within 1 to 2 km of the contact (figs. 7-9) and increases the cooling time for the pluton. However, our results should not substantially change their conclusions regarding the magnitudes and directions of fluid flux within the intrusion.

DISCUSSION

In the simulation with k = 10^{-16} m^2, temperatures increased to maxima in the *pyroxene zone* in 10,000 yr and then declined over the next 90,000 yr (fig. 7C). Beyond 350 m in the *actinolite + chlorite zone,* temperatures were within 300° to 550°C throughout the simulations, consistent with the mineral assemblage observed there. However, neither this nor any other simulation led to a gradient in temperature that accounts for the mineral zone boundary at 250 m that marks the absence of amphibolite facies minerals. This suggests that the abrupt change in texture, mineral assemblage, and inferred temperature between the *actinolite + chlorite* and *pyroxene zones* must be a consequence of the kinetics of metamorphic processes. At a given pressure, a metamorphic reaction proceeds after its equilibrium temperature has been exceeded or overstepped. The rate of reaction is limited by the slowest among a set of reaction mechanisms that include dissolution of reactant phases, transport of reactant and product species to and from reaction sites, and nucleation and growth of product phases (Fisher, 1978; Walther and Wood, 1984; 1986). One of these processes must have limited the rates of the heterogeneous reactions sufficiently that amphibolite-facies mineral assemblages did not nucleate or grow. After discussing the magnitude of the temperature overstep at 250 m, we examine the roles of transport, dissolution and growth, and nucleation in the development of the boundary between the *pyroxene* and *actinolite + chlorite zones.*

Magnitude of Temperature Overstepping

At 250 m from the contact, where the maximum oversteps are to be expected, the mineral assemblage of the *actinolite + chlorite zone* records a maximum temperature of 550°C. Temperature maxima in the simulations were strongly dependent on permeability (figs. 7 and 8). Figure 10A shows simulated temperatures as a function of time at 250 m from the contact. The maximum temperatures at this distance increased with decreasing permeability in the simulations. For $k = 10^{-16}$ m^2, the rocks at 250 m in the simulations experienced temperatures in excess of 550°C from 4000 to ~30,000 yr after emplacement. The extent and duration of overstep decreased drastically with slight increases in permeability, such that temperatures do not reach 550°C above $k \sim 3 \times 10^{-16}$ m^2. The predicted magnitudes of overstepping of 550°C at 250 m are shown in figure 10B. The maximum temperature during the simulations for $k = 10^{-16}$ m^2 was 633°C, an 83°C overstep. The maximum temperature for pure conduction corresponds to an overstep of 139°C.

The Rate Limiting Step

Transport.—In epithermal environments like the Skaergaard intrusion, contact metamorphism is typically characterized by large fluid fluxes ($\geq 10^{-9}$ g cm^{-2} s^{-1}; for example, Norton and Knight, 1977; Norton and Taylor, 1979). Walther and Wood (1984) showed that for mineral solubilities typical of metamorphic fluids, fluxes of these magnitudes preclude control of metamorphic reactions by transport of reactant and product species. Oxygen isotope compositions in the *pyroxene zone* suggest cumulative H_2O fluxes of 3.6 to 4.0 $\times 10^3$ mol cm^{-2} during metamorphism (Manning and Bird, 1993), or $\sim 2 \times 10^{-7}$ g cm^{-2} s^{-1} when averaged over the 10,000 yr period of heating. These fluxes are significant in that whole-rock $^{18}O/^{16}O$ provides a measure of flow in the grain boundary regions of rock matrices, where hornblende-forming reactions should have occurred. Our simulations for permeabilities of 10^{-16} m^2 gave similar fluxes and cumulative fluxes for the prograde event. Because fluxes associated with prograde metamorphism are about one hundred times greater than Walther and Wood's (1984) critical value of $\sim 10^{-9}$ g cm^{-2} s^{-1}, transport was probably sufficiently rapid that it did not limit reaction rates, even if solubilities of aqueous species were lower than those they used.

If transport was not rate limiting, then low rates of either dissolution, nucleation, or growth led to the boundary between the *actinolite + chlorite* and *pyroxene zones*. The extent to which these processes may have limited reaction rates depends on the nature of the metamorphic reactions. Metamorphism is commonly assumed to be progressive, such that high-grade assemblages formed from successively lower grade assemblages. Progressive metamorphism of the Skaergaard aureole would require that the *pyroxene zone* minerals formed from amphibolite-facies precursors. The boundary at 250 m would therefore correspond to the outer-

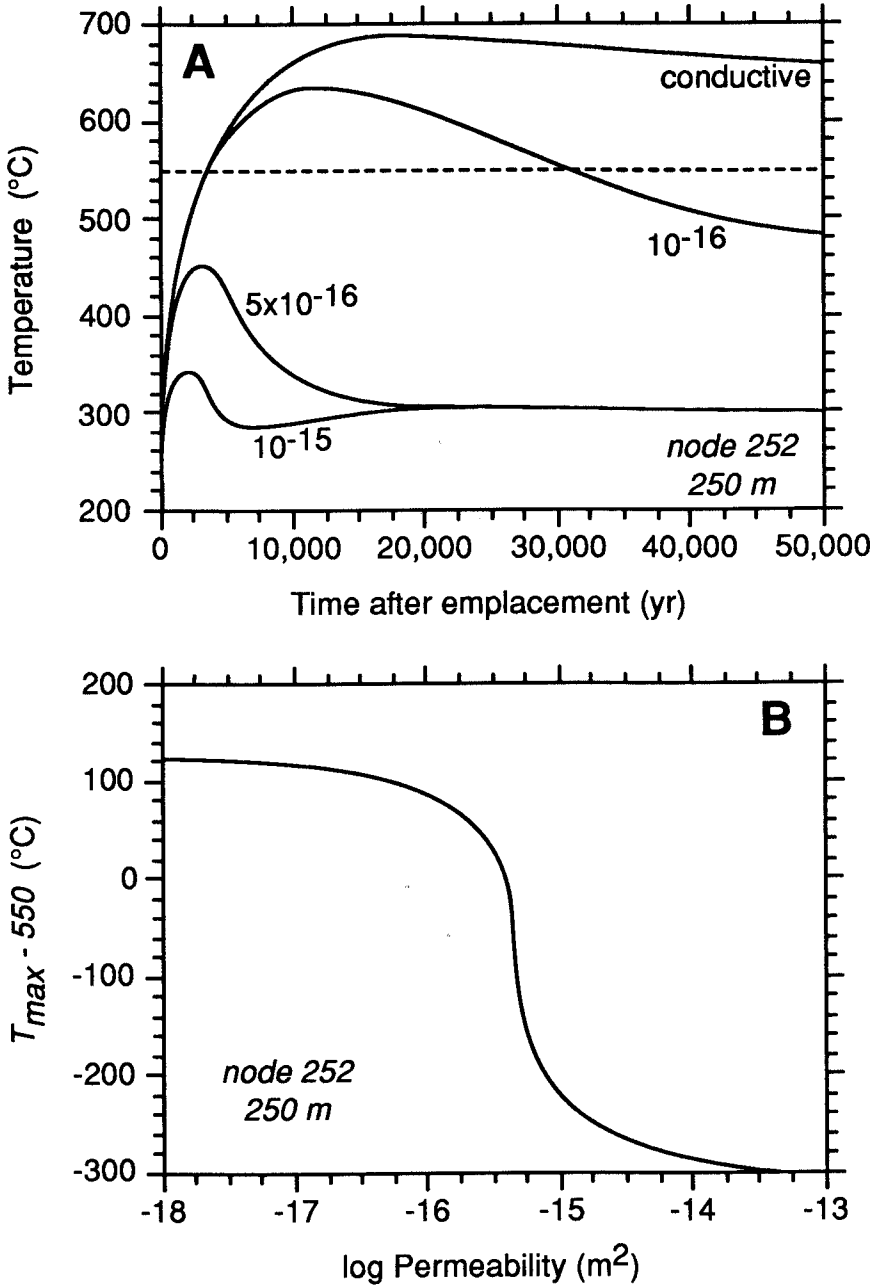

Fig. 10(A) Temperature versus time for model permeabilities for node at 250 m from the contact (node 252, fig. 4B), which corresponds to the boundary between the *pyroxene* and *actinolite + chlorite zones*. The dashed line illustrates the temperature above which hornblende-bearing assemblages are expected. (B) The difference between maximum simulated temperature and 550°C (T_{max} – 550°C) versus log permeability for the same locality in the aureole.

most limits of **both** *pyroxene zone* minerals and amphibolite-facies minerals, an improbable coincidence. The absence of hornblende in the aureole thus argues against progressive metamorphism. However, there is no way of knowing whether *pyroxene zone* minerals were preceded by precursors of even lower grade, such as *actinolite + chlorite zone* minerals, or whether all metamorphic minerals formed directly from fresh basalt. In the first scenario, hornblende would have failed to form from an assemblage of relict igneous minerals and metamorphic minerals of the greenschist facies. Alternatively, in the absence of low-temperature precursors, hornblende failed to form via hydration of the igneous minerals alone. In either case, the absence of hornblende must have resulted from (1) low rates of the dissolution or growth of reacting minerals or (2) low rates of the nucleation of hornblende.

Dissolution and growth.—If hornblende nucleation was not rate limiting, then the dissolution or growth of one of the phases participating in the hornblende-forming reactions must account for the observed pattern of mineral zones. Hornblende formation may be represented by a number of different overall reactions. For example, in the model basaltic system Na_2O–CaO–MgO–Al_2O_3–SiO_2 –H_2O, the formation of the hornblende analogue pargasite in the presence of relict igneous and greenschist-facies minerals could be represented by

$$\underset{\text{clinochlore}}{Mg_5Al_2Si_3O_{10}(OH)_8} + \underset{\text{diopside}}{3CaMgSi_2O_6} + [\underset{\text{plagioclase}}{2NaAlSi_3O_8 + CaAl_2Si_2O_8}] \rightarrow \underset{\text{pargasite}}{2NaCa_2Mg_4Al_3Si_6O_{22}(OH)_2} + \underset{\text{quartz}}{5SiO_2} + 2H_2O \quad (4)$$

Alternatively, hornblende formation from relict igneous minerals alone might take the form

$$[\underset{\text{plagioclase}}{NaAlSi_3O_8 + CaAl_2Si_2O_8}] + [\underset{\text{augite}}{CaMgSi_2O_6 + 3MgSiO_3}] + H_2O \rightarrow \underset{\text{pargasite}}{NaCa_2Mg_4Al_3Si_6O_{22}(OH)_2} + \underset{\text{quartz}}{4SiO_2} \quad (5)$$

Reactions other than (4) and (5) could also be written, but regardless of the identity of the overall reaction, hornblende formation would have been the result of a set of elementary dissolution and growth reactions at the surfaces of participating minerals. Clues as to the elementary reaction potentially responsible for limiting dissolution and growth exist in the textures, compositions, and oxygen isotope ratios in the *actinolite + chlorite zone*. The presence of partially altered igneous clinopyroxene and plagioclase point to these phases as candidates. Their major-element compositions reflect magmatic rather than metamorphic conditions beyond 250 m from the contact (Manning and Bird, 1993). Studies of the

oxygen isotope geochemistry of mafic rocks have found that both clinopyroxene and plagioclase may have only partially exchanged, whereas secondary minerals more nearly reflect isotopic equilibrium (Forester and Taylor, 1976, 1977; Taylor and Forester, 1979; Stakes, Taylor, and Fisher, 1984; Stakes and Taylor, 1992). However, these studies and others (Gregory and Taylor, 1981; Ito and Clayton, 1983; Fehlhaber and Bird, 1991) showed that pyroxene is substantially more refractory with respect to oxygen exchange than plagioclase. Also, rate constants for the dissolution of albite in H_2O are several orders of magnitude lower than those of diopside at 550°C (Murphy and Helgeson, 1989). Thus, if dissolution or growth was rate limiting, the dissolution of augite was probably the slowest of the participating elementary reactions.

Murphy and Helgeson (1989) used the low-temperature experiments of Schott, Berner, and Sjöberg (1981) to derive expressions for the rate of clinopyroxene hydrolysis as a function of temperature. Because of the difficulties in accounting for adsorption and activated complexes, Murphy and Helgeson (1989) retrieved "operational" rate constants (**k′**, in mol cm^{-2} s^{-1}). For the intermediate pH likely in the dilute aqueous fluids of the Skaergaard aureole (Manning, 1989), **k′** is related to the operational rate of diopside dissolution, r', through

$$r' = -\frac{1}{\bar{s}}\frac{dn}{dt} = \mathbf{k}'a_{H^+}^{0.5}\left(1 - \exp\left(\frac{-\mathbf{A}}{2RT}\right)\right) \tag{6}$$

(Murphy and Helgeson, 1989, eq 17 and table 1), where $\bar{s}$ is the total surface area of the reacting mineral (cm^2), n is moles of the reacting mineral, a_{H^+} is the activity of the hydrogen ion in the fluid phase, **A** is the chemical affinity (J $mole^{-1}$), R is the gas constant, and T is absolute temperature.

Eq (6) shows that for a given total surface area and fluid composition, the operational rate of diopside dissolution is a function of **A** as well as **k′**. The chemical affinity describes the magnitude of the deviation from equilibrium and can be evaluated by recognizing that the absence of hornblende reflects overstepping of the equilibrium temperature of formation of ~550°C for the bulk composition and conditions of the Skaergaard aureole. As temperatures increased beyond 550°C, the fluid phase likely maintained local equilibrium with all minerals other than the more refractory clinopyroxene. The sum of the heat capacities of the various elementary reactions leading to hornblende growth was probably small, so near equilibrium,

$$\mathbf{A} = -\Delta G_r = \Delta S_r(T - T_{eq}) \tag{7}$$

where ΔG_r and ΔS_r are the molar Gibbs free energy and entropy of reaction and T_{eq} is the equilibrium temperature of the reaction in Kelvins.

For spherical crystals, eqs (6) and (7) can be combined to give the operational rate of diopside dissolution expressed in terms of radius r:

$$\frac{dr}{dt} = 66.09\mathbf{k}'a_{H^+}^{0.5}(1 - \exp[-\Delta S_r(T - T_{eq})/2RT]) \quad (8)$$

(compare, Walther and Wood, 1984), where the factor 66.09 is the molar volume of diopside (Helgeson and others, 1978). Eq (8) allows a first-order estimate of the extent to which clinopyroxene dissolution rates can account for the distribution of mineral zones in the Skaergaard aureole.

Assuming neutral pH (~5.5 at 550°-650°C, 2 kb) and diopside spheres of 0.1 cm radius, which exceeds the average long dimension of relict clinopyroxenes by about a factor of ten, we evaluated the integrated form of eq (8) at 1000 yr intervals using the temperature-time history for $k = 10^{-16}$ m^2 (fig. 10A) and a range in entropies of the overall reaction. Figure 11 shows the variation in radius of a diopside sphere with time for different values of ΔS_r. If differences in entropy between reactants and products were as low as 0.04 J mol^{-1}K^{-1}, diopside spheres would have completely dissolved in <2000 yr after 550°C was exceeded. This is in accord with the calculations of Walther and Wood (1984), which were

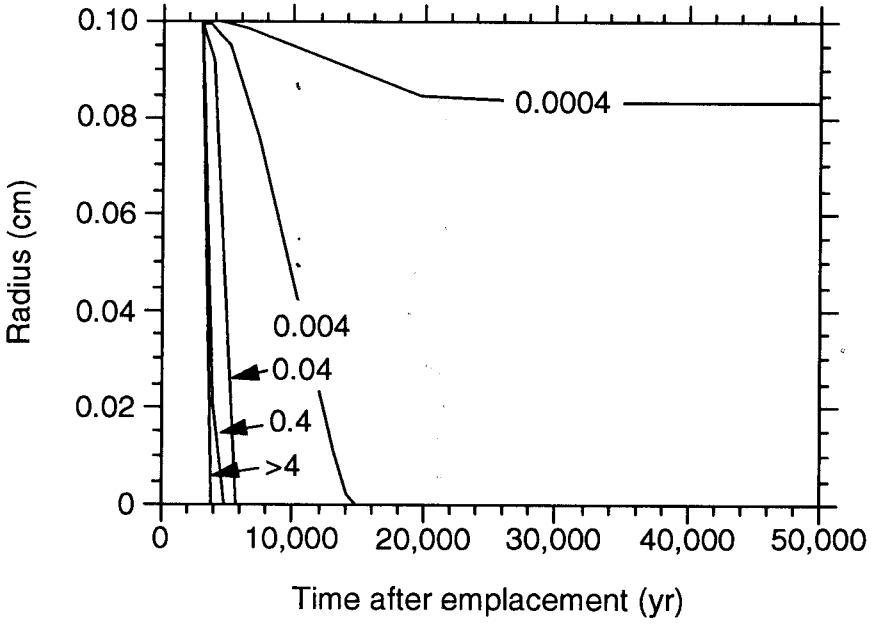

Fig. 11. Radius of spherical diopside crystals as a function of time for different values of ΔS_r in J mol^{-1}K^{-1}, computed from eq (11) using the temperature-time history for $k = 10^{-16}$ m^2 at 250 m from the contact.

based on different rate constants (Wood and Walther, 1983). Only if $\Delta S_r < 0.002$ J mol^{-1}K^{-1} could diopside dissolution have been rate limiting, given the preferred temperature-time history. The entropy differences between reactants and products in reactions (4) and (5) serve as analogues for the actual overall reaction that might have occurred at 250 m had hornblende grown. The identities and stoichiometries of participating phases may have been different, but the entropy differences between actual reactants and products can be taken as similar in magnitude to those in the model reactions. Because the absolute values of ΔS_r for reactions (4) and (5) are 175 and 29 J mol^{-1}K^{-1}, respectively (Helgeson and others, 1978), and because only small differences in entropies arise from accounting for solid solutions, clinopyroxene dissolution could not have been rate limiting given the assumptions adopted here.

Our assumptions were conservative. More acidic solutions and smaller crystals would increase the amount of diopside dissolved. Moreover, diopside dissolution was assumed to proceed only above 550°C, which also leads to a minimum estimate of the amount of diopside dissolved. Surface areas are not constrained, but for diopside dissolution to limit overall reaction rates would have to have been higher by more than three orders of magnitude than those used. Increased model permeabilities would decrease the magnitude and duration of the temperature overstep; however, even for oversteps as low as several degrees, diopside dissolution would have been sufficiently rapid that crystals 0.2 cm in diameter would have dissolved completely in hundreds of years. Finally, we note that the mineral zones record the absence of hornblende, not the incomplete reaction to hornblende-bearing assemblages. This implies that nucleation, not dissolution or growth, limited reaction rates in this portion of the contact aureole.

Hornblende nucleation.—Though it is commonly asserted that nucleation is not rate limiting during metamorphism (Walther and Wood, 1984, 1986), experimental studies show that nucleation rates of calcic amphiboles are exceptionally slow (Jenkins, 1988; Dachs and Metz, 1988; Cho and Ernst, 1991). The extent to which reactions forming hornblende might be overstepped before this phase nucleates can be assessed using the equation for nucleation rate, $\dot{n}$, in a homogeneous medium applied to polygranular aggregates (McLean, 1965; Ridley, 1985; Rubie and Thompson, 1985; Ridley and Thompson, 1986):

$$\dot{n} = K \exp\left(\frac{-16\pi\gamma^3}{3\Delta\bar{G}_r^2 k_B T}\right) \tag{9}$$

where γ is the interfacial free energy (J m^{-2}), k_B is Boltzmann's constant, and ΔG_r is the Gibbs free energy per m^3 of the product assemblage (J m^{-3}), which is related to the volumetric entropy difference between

reactant and product phases, $\Delta\tilde{S}_r$ in J m^{-3} K^{-1}, by an equation similar to (7):

$$-\Delta\tilde{G}_r = \Delta\tilde{S}_r(T - T_{eq}) \tag{10}$$

Here $T - T_{eq}$ is the overstep of the equilibrium temperature required to cause product minerals to nucleate at the rate $\dot{n}$. The constant K in (9) is related to the activation energy for nucleation, E_A, by

$$K = N\nu \exp\left(\frac{-E_A}{RT}\right) \tag{11}$$

(Fyfe, Turner, and Verhoogen, 1958), where N is Avogadro's Number times the number of moles of products per m^3, and ν is the atomic vibration frequency.

Ridley and Thompson (1986) suggested that nucleation rates in excess of 10^{-7} s^{-1} m^{-3} (~ 1 yr^{-1} m^{-3}) are required to form observable quantities of a mineral. Activation energies for nucleation are poorly known but should equal or exceed activation energies for diffusion in the phase of interest or in similar phases. The activation energy for diffusion of argon in hornblende is ~270 kJ mol^{-1} (McDougall and Harrison, 1988); that for interdiffusion of Ca and Mg in diopside is ~360 kJ mol^{-1} (Brady and McCallister, 1983). These values fall within estimates for dehydration and decarbonation reactions of ~100 to ~750 kJ mol^{-1} (Kridelbaugh, 1973; Wegner and Ernst, 1983; Chermak and Rimstidt, 1990). Assuming as a first approximation an activation energy of 300 kJ mol^{-1} for $\dot{n} = 10^{-7}$ s^{-1} m^{-3}, eqs (9) through (11) can be combined to evaluate temperature oversteps as a function of entropy differences and interfacial free energies.

Figure 12 shows $T - T_{eq}$ versus interfacial free energy for relevant metamorphic reactions calculated using the thermodynamic data of Helgeson and others (1978). Variations in temperature overstep for reactions having $\Delta\tilde{S}_r$ of 50, 250, and 500 kJ m^{-3} K^{-1} are shown with dashed lines. The lower entropy changes are equivalent to the solid-solid equilibria andalusite = sillimanite and kyanite = sillimanite, respectively, at 550° to 650°C. The large $\Delta\tilde{S}_r$ value corresponds to that for

$$\underset{\text{muscovite}}{KAl_3Si_3O_{10}(OH)_2} + \underset{\text{quartz}}{SiO_2} = \underset{\text{K feldspar}}{KAlSi_3O_8} + \underset{\text{sillimanite}}{Al_2SiO_5} + H_2O \tag{12}$$

Figure 12 shows that at constant γ, $T - T_{eq}$ increases with decreasing $\Delta\tilde{S}_r$. At constant $\Delta\tilde{S}_r$, the overstep of equilibrium temperature increases with increasing interfacial free energies.

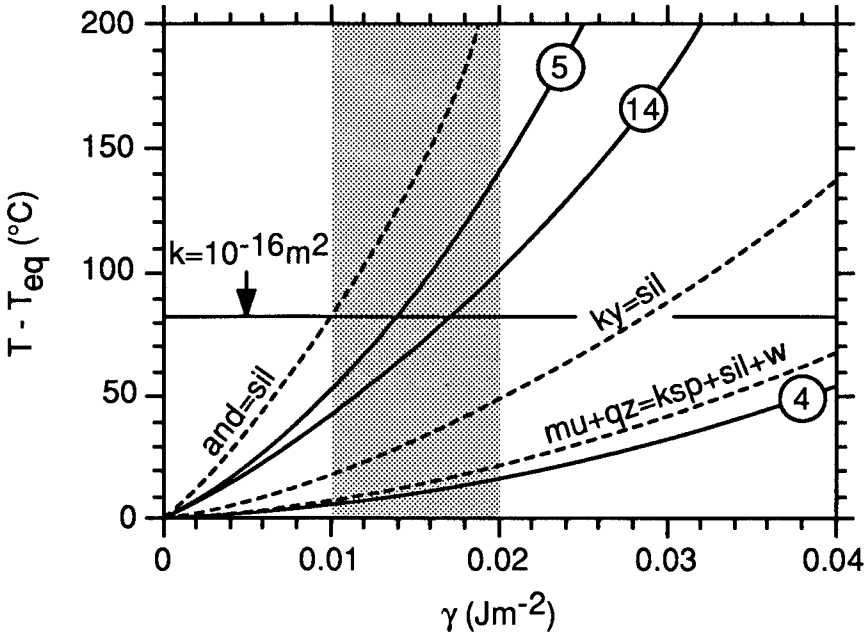

Fig. 12. Temperature overstep versus interfacial free energy for different metamorphic reactions. The solid curves labeled 4, 5, and 14 are eqs (4), (5), and (14) in the text. The horizontal line denotes the temperature oversteps calculated for $k = 10^{-16}$ m^2. Stippling depicts values of interfacial free energy for geologic materials (see text).

Dachs and Metz (1988) experimentally investigated the reaction

$$\underset{\text{tremolite}}{Ca_2Mg_5Si_8O_{22}(OH)_2} + 3\underset{\text{calcite}}{CaCO_3} + 2\underset{\text{quartz}}{SiO_2} \rightarrow 5\underset{\text{diopside}}{CaMgSi_2O_6} + 3CO_2 + H_2O \quad (13)$$

at 2 and 5 kb. The difference in entropy between reactant and product phases at the conditions of their experiments is similar to reaction (12), using the assumptions outlined above. Dachs and Metz (1988) were best able to characterize the magnitude of $T - T_{eq}$ for diopside nucleation in their 5 kb experiments, in which they observed oversteps of 30° to 60°C. They noted that the probable range of values of γ in crystalline rocks is 0.01 to 0.02 J m^{-2} (Porter and Easterling, 1981; Ridley and Thompson, 1986), about 20 to 25 times lower than γ for quartz-water and kaolinite-water (Parks, 1984; Steefel and Van Cappellen, 1990). With the assumptions adopted here, the temperature oversteps predicted are at the lower limit of the oversteps observed by Dachs and Metz (1988) at $\gamma = 0.02$ J m^{-2} (fig. 12). If a larger E_A were assumed (for example, 500 kJ mol^{-1}),

oversteps of 30° to 60°C would be within the geologically reasonable values of γ shown in the figure.

The relationship between $T - T_{eq}$ and γ for hornblende-forming reactions can be assessed using reactions (4) and (5). Reaction (4) illustrates the formation of pargasite from both greenschist-facies and relict igneous minerals. The value of $\Delta\tilde{S}_r$ at 550°C is larger than that for muscovite dehydration in the presence of quartz (2340 kJ $m^{-3}K^{-1}$). Figure 12 illustrates that temperature oversteps of only 5° to 20°C would occur for hornblende nucleation at 10^{-7} yr^{-1} m^{-3}. Conversely, the entropy difference between reactants and products in (5), which models hornblende formation solely from an anhydrous igneous assemblage, is 80 kJ $m^{-3}K^{-1}$ at 550°C, a value nearer to solid-solid reactions than hydration-dehydration reactions. Figure 12 shows that for γ between 0.01 and 0.02 J m^{-2}, temperature oversteps in excess of 50°C will be required to yield nucleation rates sufficient to form hornblende at the $\Delta\tilde{S}_r$ of reaction (5).

Hornblende in mafic rocks is typically a mixture of the calcic amphibole endmembers tremolite, pargasite, and tschermakite and increases in ^{IV}Al content with increasing temperature (Liou, Kuniyoshi, and Ito, 1974; Spear, 1981; Robinson and others, 1982; Moody, Meyers, and Jenkins, 1983). The effect of nucleation of amphibole along the tremolite-pargasite join can be evaluated by comparing (5) with

$$\underset{\text{pargasite}}{NaCa_2Mg_4Al_3Si_6O_{22}(OH)_2} + \underset{\text{diopside}}{CaMgSi_2O_6} + \underset{\text{quartz}}{5SiO_2} = \underset{\text{tremolite}}{Ca_2Mg_5Si_8O_{22}(OH)_2} + \underset{\text{albite}}{NaAlSi_3O_8} + \underset{\text{anorthite}}{CaAl_2Si_2O_8} \quad (14)$$

which models the continuous exchange of components between amphibole endmembers in the presence of relict igneous phases in a basalt. The value of $\Delta\tilde{S}_r$ for (14) is 120 kJ $m^{-3}K^{-1}$ at 550°C. This shows that the change in entropy caused by adding tremolite component to pargasite is also similar in magnitude to the entropy difference between the aluminosilicates, suggesting that the composition of amphibole along the tremolite-pargasite join will not cause important differences in the magnitude of $\Delta\tilde{S}_r$ of the overall hornblende-forming reaction.

In the simulation that best reproduces the inferred metamorphic temperatures and fluid fluxes ($k = 10^{-16}$ m^2), the magnitude of overstepping of the 550°C temperature at which hornblende should have formed was ~80°C (fig. 10). This is shown in figure 12 by the horizontal line. Within the range of likely γ, the simulated overstep intersects the curve for reaction (5) but is substantially greater than that which would be consistent with reaction (4). We assumed $E_A = 300$ kJ mol^{-1}, but this quantity is poorly known and is probably a minimum. If E_A were increased to 500 kJ mol^{-1}, predicted oversteps would be >70°C for

reaction (5) but $<30°C$ for reaction (4) within the probable range for geologic materials.

Figure 12 shows that hornblende nucleation could have limited reaction rates and led to the missing mineral zones if the protolith was an unaltered basaltic mineral assemblage (reaction 5). If extensive replacement of relict igneous minerals by greenschist facies assemblages had occurred in the early stages of heating below 550°C, the entropy change associated with the dehydration of this assemblage above 550°C (reaction 4) would have been so great that hornblende should have nucleated at the critical rate after oversteps of only 5° to 20°C. Moreover, precursor phases such as actinolite and chlorite should have provided ample nucleation sites, further lowering temperature oversteps before critical rates of hornblende nucleation were attained. As hornblende is not observed in the aureole, and as the thermometry and inferred fluid fluxes require the larger oversteps consistent with lower entropy reactions, we conclude that hornblende nucleation rates were rate limiting and that the basalt protolith was virtually unaltered. This is not implausible: 550°C was exceeded at 250 m from the contact after only ~ 3000 yr in the simulation in which $k = 10^{-16}$ m^2, and fluid fluxes were low during this time. Limiting reactions through slow hornblende nucleation rates in an unaltered protolith explains the distribution of mineral zones by allowing reaction to *pyroxene zone* assemblages during prograde heating within 250 m from the contact but preventing reaction to hornblende-bearing assemblages beyond this distance. After peak temperatures were attained, *actinolite + chlorite zone* assemblages nucleated and grew when temperatures had cooled to less than $\sim 550°C$. Thus, the two mineral zones did not form at the same time.

CONCLUDING REMARKS

Comparison of simulations with thermometry and oxygen isotope geochemistry suggests that time- and volume-averaged permeabilities of the contact aureole were $\sim 10^{-16}$ m^2 and that the absence of amphibolite-facies mineral assemblages in the aureole is a kinetic feature. Using the simulation results for this permeability and data for clinopyroxene dissolution rates, we conclude that neither transport nor dissolution and growth reactions were rate limiting. Rather, our analysis suggests that low rates of hornblende nucleation best explain the distribution of mineral zones in the Skaergaard's aureole. If this is so, how can these observations aid comparisons of contact aureoles in mafic rocks elsewhere?

Like the Skaergaard's contact aureole, metamorphosed Tertiary basalts hosting gabbros on the Isle of Skye, Scotland, lack an amphibolite-facies mineral zone and had a relatively unaltered basalt protolith (Almond, 1964; Ferry, Mutti, and Zuccala, 1987). Ferry, Mutti, and Zuccala (1987) described greenschist-facies mineral assemblages (*amphibole zone*) locally in contact with high-grade metabasalts with granoblastic-polygonal textures and the silicate mineral assemblage orthopyroxene + clino-

pyroxene + olivine + plagioclase (*orthopyroxene-olivine zone*). The *orthopyroxene-olivine zone* is commonly absent, and the *amphibole zone* is in direct contact with the gabbros around most of the intrusion. The absence of high grade mineral assemblages from most of this aureole strongly implies that the rocks of the *amphibole zone* experienced temperature oversteps of similar or greater magnitude than analogous rocks from the Skaergaard aureole. About half the *amphibole zone* rocks contain aluminous calcic amphibole (Ferry, Mutti, and Zuccala, 1987), but its modal abundance is vanishingly small (J. M. Ferry, personal communication). Assuming that it is metamorphic rather than magmatic in origin, the low modal abundance implies that nucleation rates or temperature oversteps were somewhat higher than in the Skaergaard aureole, but neither was sufficient to make hornblende-bearing assemblages as pervasive as they should have been had equilibrium been obtained. Conversely, the contact metamorphosed Karmutsen basalts of Vancouver Island, British Columbia, are marked by well-developed hornblende-bearing assemblages between mineral zones analogous to the *pyroxene* and *actinolite + chlorite zones* of the Skaergaard aureole (Kuniyoshi and Liou, 1976a). Clearly, hornblende nucleation rates were sufficient at this locality to form the typical progression of metabasalt mineral zones.

A key difference between the protoliths in the North Atlantic Tertiary province and on Vancouver Island is that the latter were subjected to a regional zeolite-facies metamorphic event prior to contact metamorphism (Kuniyoshi and Liou, 1976b), which may have more extensively altered these basalts. We suggest that the extent of hydration prior to contact metamorphism exerts a primary control on the nucleation of hornblende in mafic lithologies. In the previously metamorphosed Karmutsen basalts, metamorphic reactions appear to have proceeded by a progressive series of dehydration reactions. As shown in figure 12, dehydration reactions are likely to result in small oversteps, favoring progressive metamorphism in which each mineral zone develops successively at a given distance from the contact. If progressive metamorphism led to the formation of actinolite-bearing mineral assemblages prior to peak hornblende-bearing assemblages, favorable nucleation sites involving actinolite may have further facilitated hornblende formation, much as seed crystals enhance hornblende nucleation and growth in experimental systems. In contrast, the metamorphism of fresh, relatively anhydrous basalts does not involve dehydration reactions and is thus more likely to be associated with large temperature oversteps such as those implied by the distribution of mineral zones in the North Atlantic Tertiary province. Because metamorphism in this scenario is not progressive, the lack of favorable nucleation sites in the form of precursor phases may help to impede hornblende nucleation.

The missing mineral zones in the contact aureoles of the North Atlantic Tertiary province are kinetic features that are likely related to the low entropy changes associated with hornblende nucleation reac-

tions. They represent extreme examples of kinetically controlled isograds and are features to be expected in mafic lithologies when protoliths are unaltered and metamorphism is not progressive. We have shown that metamorphic equilibria involving an aluminous calcic amphibole and pyroxene, plagioclase, and quartz may involve entropy changes similar to those of equilibria among aluminosilicates. The well-known problem of overstepping sillimanite-nucleation reactions in pelitic contact aureoles thus appears to have an analogue in hornblende-forming reactions in mafic contact aureoles.

ACKNOWLEDGMENTS

We thank J. Ferry and D. Waters for helpful reviews. M. Donato, D. Rothstein, E. Rowan, and M. Scholl improved early drafts of the manuscript. The numerical simulations were initiated while the senior author was at the U.S. Geological Survey, Menlo Park (NSF EAR-8615714 to Steven R. Bohlen). Portions of this study were also supported by NSF grants EAR-9104288 to Manning and EAR-8606256 and EAR-8803754 to Bird. This work benefitted from field support from Platinova Resources, the Geological Survey of Greenland, and the Geological Society of America.

APPENDIX 1

Compositions of Ca-rich pyroxene and estimated temperatures

Sample	Distance from Contact (m)	Analysis number	Analyzed X_{Ca}	Analyzed X_{Mg}	Projected X_{Ca}	Projected X_{Mg}	Temperature (°C)
1118	390	14	0.3822	0.4940	0.3442	0.5244	1083
		17	0.3809	0.5014	0.3446	0.5201	1078
		18	0.3677	0.4824	0.3363	0.5063	1064
		19	0.3765	0.4958	0.3429	0.5225	1081
1133	249	27	0.3805	0.4247	0.3428	0.4505	1006
		28	0.3791	0.4645	0.3247	0.5052	1061
		29	0.3903	0.4848	0.3676	0.5029	1052
		31	0.3801	0.4510	0.3678	0.4599	1002
		34	0.4044	0.4250	0.3628	0.4546	1001
		35	0.3879	0.4428	0.3469	0.4724	1028
1345	240	2	0.4539	0.3777	0.4463	0.3829	707
		4	0.4348	0.3904	0.4180	0.4020	842
		5	0.4492	0.3997	0.4350	0.4100	787
		6	0.4534	0.4085	0.4433	0.4160	754
		7	0.4487	0.4049	0.4340	0.4157	797
		8	0.4413	0.3874	0.4312	0.3943	787
		10	0.4568	0.4014	0.4461	0.4093	732
		11	0.4611	0.4201	0.4473	0.4308	750
		12	0.4411	0.4112	0.4348	0.4158	794
		13	0.4469	0.4043	0.4394	0.4097	766
		14	0.4500	0.3912	0.4446	0.3950	726
		15	0.4499	0.3883	0.4406	0.3949	746
		16	0.4490	0.4012	0.4357	0.4108	785
		17	0.4435	0.3845	0.4323	0.3932	781
		18	0.4235	0.3954	0.4134	0.4023	856
		19	0.3648	0.4001	0.3582	0.4043	953
		20	0.4474	0.3942	0.4357	0.4026	776
		21	0.3774	0.4285	0.3626	0.4386	984
		25	0.4388	0.3892	0.4235	0.3998	821
1323	240	3	0.4409	0.3982	0.4283	0.4071	811
		4	0.4563	0.4112	0.4484	0.4171	728
		5	0.4487	0.3848	0.4358	0.3938	767
		6	0.4351	0.3902	0.4188	0.4014	839
		7	0.4357	0.3911	0.4268	0.3973	807
		10	0.4305	0.3820	0.4189	0.3898	827
		12	0.4236	0.4017	0.4141	0.4084	860
1183	219	39	0.4537	0.3926	0.4405	0.4020	753
		40	0.4575	0.3839	0.4458	0.3922	718
		41	0.4572	0.3963	0.4337	0.4135	796
		42	0.4508	0.3882	0.4360	0.3986	771
		43	0.4509	0.3775	0.4370	0.3870	756
		44	0.4548	0.3912	0.4366	0.4042	774
		45	0.4689	0.3654	0.4501	0.3783	683
		46	0.4387	0.3878	0.4271	0.3958	804
		47	0.4548	0.3896	0.4346	0.4039	782
		48	0.4539	0.3890	0.4387	0.3998	760

APPENDIX 1

(continued)

Sample	Distance from Contact (m)	Analysis number	Analyzed X_{Ca}	Analyzed X_{Mg}	Projected X_{Ca}	Projected X_{Mg}	Temperature (°C)
1184	210	a1	0.4500	0.3932	0.4361	0.4031	775
		a8	0.4579	0.3631	0.4473	0.3702	693
		b1	0.4452	0.3924	0.4253	0.4065	822
		b3	0.4313	0.3928	0.4129	0.4055	861
1321	155	4	0.4523	0.4158	0.4373	0.4271	796
		5	0.4508	0.4025	0.4234	0.4225	846
		6	0.4521	0.4066	0.4369	0.4179	787
1169	133	1	0.4373	0.3726	0.4255	0.3804	796
		2	0.4318	0.3716	0.4057	0.3887	864
		7	0.4387	0.3776	0.4240	0.3865	807
1165	125	2	0.4508	0.3888	0.4338	0.4009	783
		4	0.4421	0.3858	0.4288	0.3950	797
		13	0.4419	0.3808	0.4291	0.3896	791
		18	0.4393	0.3895	0.4238	0.4002	821
844O	69	7	0.4499	0.2956	0.4280	0.3741	782
		9	0.4499	0.2993	0.4187	0.3163	771
		13	0.4224	0.3525	0.4006	0.3658	856
		14	0.4231	0.3499	0.4013	0.3631	852
		15a	0.4440	0.3227	0.4202	0.3366	780
		17	0.4356	0.3613	0.4078	0.3791	850
1340	54	5	0.4278	0.3821	0.4139	0.3914	847
		6	0.4380	0.3864	0.4260	0.3946	807
		9	0.4367	0.3741	0.4239	0.3826	804
1185T	32	b0.3	0.4139	0.4142	0.3909	0.4304	939
		b0.4	0.4341	0.3913	0.4182	0.4023	842
		b2.2	0.4324	0.3883	0.4174	0.3985	840
		b2.3	0.4314	0.3849	0.4145	0.3963	847
		b3.3	0.4310	0.3866	0.4023	0.4061	889
		b4	0.4396	0.3880	0.4274	0.3965	804
		b5.2	0.4316	0.3863	0.4123	0.3994	857
		b6	0.4331	0.3848	0.4112	0.3997	860
		b7.1	0.4395	0.3955	0.4199	0.4094	843
		b7.2	0.4330	0.3990	0.4181	0.4095	849
		b8	0.4444	0.3920	0.4268	0.4044	814
		b9	0.4261	0.4023	0.4011	0.4199	906
		b10	0.4458	0.3919	0.4315	0.4020	793
		b11	0.4483	0.3885	0.4320	0.4000	789
		c1	0.4331	0.3963	0.4130	0.4104	866
		c3	0.4368	0.3924	0.4254	0.4003	815
		c5	0.4237	0.3996	0.4091	0.4098	876
		c6	0.4371	0.3835	0.4194	0.3995	835
1185K	3	4	0.4089	0.4089	0.3945	0.4189	919
		7	0.4434	0.4038	0.4278	0.4151	821
		8	0.4245	0.4145	0.4041	0.4292	910
		9	0.3960	0.4163	0.3790	0.4280	955

Sample locations given in figure 2. Pyroxene compositions were determined by electron microprobe analysis using 15 kv accelerating potential, 15 na on Faraday cup, focused (~3 μm) beam, and 30 sec. counting times. Well-characterized silicates and oxides were employed as standards, and oxide sums were calculated with a Bence-Albee (1968) matrix-correction algorithm (Chambers, 1985). Projected mole fractions calculated using equations of Lindsley and Anderson (1983). Temperatures calculated using equations of Anderson, Lindsley, and Davidson (1993) assuming 2 kb. Complete analyses available from C. E. Manning.

References

Almond, D. C., 1964, Metamorphism of Tertiary lavas in Strathaird, Skye: Transactions of the Royal Society of Edinburgh, v. 45, p. 413–435.

Anderson, D. J., Lindsley, D. H., and Davidson, P. M., 1993, QUILF: a PASCAL program to assess equilibria among Fe-Mg-Ti oxides, pyroxenes, olivine, and quartz: Computers & Geosciences, in press.

Andrew, A. S., 1984, P-T-X(CO_2) conditions in mafic and calc-silicate hornfelses from Oberon, New South Wales, Australia: Journal of Metamorphic Geology, v. 2, p. 143–163.

Andrew, A. S., and O'Neil, J. R., 1988, Role of fluids during contact metamorphism: stable isotope evidence from the Rockley Volcanics, eastern Australia: American Journal of Science, v. 288-A, p. 490–511.

Barton, M. D., Staude, J-M., Snow, E. A., and Johnson, D. A., 1991, Aureole systematics, *in* Kerrick, D. M., editor, Contact Metamorphism: Reviews in Mineralogy, v. 26, p. 723–847.

Baumgartner, L. P., and Rumble, D., III, 1988, Transport of stable isotopes: I: Development of a kinetic continuum theory for stable isotope transport: Contributions to Mineralogy and Petrology, v. 98, p. 417–430.

Bence, A. E., and Albee, A. L., 1968, Empirical correction factors for the electron microanalysis of silicates and oxides: Journal of Geology, v. 76, p. 382–403.

Bickle, M. J., and McKenzie, D., 1987, The transport of heat and matter by fluids during metamorphism: Contributions to Mineralogy and Petrology, v. 95, p. 384–392.

Bird, D. K., Manning, C. E., and Rose, N. M., 1988, Hydrothermal alteration of Tertiary layered gabbros, East Greenland: American Journal of Science, v. 288, p. 405–457.

Bird, D. K., Rogers, R. D., and Manning, C. E., 1986, Mineralized fracture systems of the Skaergaard intrusion: Meddelser om Grønland, Geoscience, v. 16, 68 p.

Bird, D. K., Rosing, M. T., Manning, C. E., and Rose, N. M., 1985, Geologic field studies of the Miki Fjord area, East Greenland: Geological Society of Denmark Bulletin, v. 34, p. 219–236.

Bird, D. K., Schiffman, P., Elders, W. A., Williams, A. E., and McDowell, S. D., 1984, Calc-silicate mineralization in active geothermal systems: Economic Geology, v. 79, p. 671–695.

Blattner, P., and Lassey, K. R., 1989, Stable isotope exchange fronts, Damköhler numbers, and fluid to rock ratios: Chemical Geology, v. 78, p. 381–392.

Bodvarsson, G. S., ms, 1982, Mathematical modeling of the behavior of geothermal systems under exploitation: Ph.D. thesis, University of California, Berkeley, California, 353 p.

Bowers, J. R., Kerrick, D. M., and Furlong, K. P., 1990, Conduction model for the thermal evolution of the Cupsuptic aureole, Maine: American Journal of Science, v. 290, p. 644–665.

Brady, J. B., and McCallister, R. H., 1983, Diffusion data for clinopyroxene from homogenization and self-diffusion experiments: American Mineralogist, v. 68, p. 95–105.

Brooks, C. K., 1980, Episodic volcanism, epeirogenesis and the formation of the North Atlantic ocean: Paleogeography Paleoclimatology Paleoecology, v. 30, p. 229–242.

Brooks, C. K., and Gleadow, A. J. W., 1979, A fission-track age for the Skaergaard intrusion and the age of the East Greenland basalts: Geology, v. 5, p. 539–540.

Brooks, C. K., and Nielsen, T. F. D., 1982a, The Phanerozoic development of the Kangerdlugssuaq area, East Greenland: Meddelser on Grønland, Geoscience, v. 9, 30 p.

———— 1982b, The East Greenland continental margin: a transition between oceanic and continental magmatism: Journal of the Geological Society of London, v. 139, p. 265–275.

Cathles, L. M., 1977, An analysis of the cooling of intrusives by ground-water convection which includes boiling: Economic Geology, v. 72, p. 804–826.

Chambers, W. F., 1985, SANDIA TASK8: a subroutined electron microprobe automation system: Sandia National Labortories Report SAND85-2037, 115 p.

Chermak, J.A., and Rimstidt, J.D., 1990, The hydrothermal transformation rate of kaolinite to muscovite/illite: Geochimica et Cosmochimica Acta, v. 54, p. 2979–2990.

Cho, M., and Ernst, W. G., 1991, An experimental determination of calcic amphibole solid solution along the join tremolite-tschermakite: American Mineralogist, v. 76, p. 985–1001.

Clark, S. P., editor, 1966, Handbook of physical constants: Geological Society of America Memoir 97, 587 p.

Dachs, E., and Metz, P., 1988, The mechanism of the reaction 1 tremolite + 3 calcite + 2 quartz = 5 diopside + 3 CO_2 + 1 H_2O: results of powder experiments: Contributions to Mineralogy and Petrology, v. 100, p. 542–551.

Davidson, P. M., 1985, Thermodynamic analysis of quadrilateral pyroxenes. Part I. Derivation of the ternary nonconvergent site-disorder model: Contributions to Mineralogy and Petrology, v. 91, p. 383–389.

Davidson, P. M., and Lindsley, D. H., 1985, Thermodynamic analysis of quadrilateral pyroxenes. Part II. Model calibration from experiments and applications to geothermometry: Contributions to Mineralogy and Petrology, v. 91, p. 390–404.

Delaney, P. T., 1988, Fortran77 programs for conductive cooling of dikes with temperature-dependent thermal properties and heats of crystallization: Computers & Geosciences, v. 14, p. 181–212.

Dipple, G. M., and Ferry, J. M., 1992, Fluid flow and stable isotopic alteration in rocks at elevated temperatures with applications to metamorphism: Geochimica et Cosmochimica Acta, v. 56, p. 3539–3550.

Fehlhaber, K., and Bird, D. K., 1991, Oxygen-isotope exchange and mineral alteration in gabbros of the Lower Layered Series, Kap Edvard Holm Complex, East Greenland: Geology, v. 19, p. 819–822.

Ferry, J. M., 1991, Dehydration and decarbonation reactions as a record of fluid infiltration, *in* Kerrick, D. M., editor, Contact Metamorphism: Reviews in Mineralogy, v. 26, p. 351–393.

Ferry, J. M., Mutti, L. J., and Zuccala, G. J., 1987, Contact metamorphism/hydrothermal alteration of Tertiary basalts from the Isle of Skye, northwest Scotland: Contributions to Mineralogy and Petrology, v. 95, p. 166–181.

Fisher, G. W., 1978, Rate laws in metamorphism: Geochimica et Cosmochimica Acta, v. 42, p. 1035–1050.

Forester, R. W., and Taylor, H. P., Jr., 1976, ^{18}O-depleted igneous rocks from the Tertiary complex of the Isle of Mull, Scotland: Earth and Planetary Science Letters, v. 32, p. 11–17.

———— 1977, $^{18}O/^{16}O$, D/H, and $^{13}C/^{12}C$ studies of the Tertiary igneous complex of Skye, Scotland: American Journal of Science, v. 277, p. 136–177.

Furlong, K. P., Hanson, R. B., and Bowers, J. R., 1991, Modeling thermal regimes, *in* Kerrick, D. M., editor, Contact Metamorphism: Reviews in Mineralogy, v. 26, p. 437–505.

Fyfe, W. S., Turner, F. J., and Verhoogen, J., 1958, Metamorphic reactions and metamorphic textures: Geological Society of America Memoir 73, 259 p.

Gregory, R. T., and Taylor, H. P., Jr., 1981, An oxygen isotope profile in a section of Cretaceous oceanic crust, Samail ophiolite, Oman: evidence for $\delta^{18}O$ buffering of the oceans by deep (>5 km) seawater-hydrothermal circulation at mid-ocean ridges: Journal of Geophysical Research, v. 86, p. 2737–2755.

Hanson, R. B., 1992, Effects of fluid production on fluid flow during regional and contact metamorphism: Journal of Metamorphic Geology, v. 10, p. 87–97.

Hanson, R. B., Sorenson, S. S., Barton, M. D., and Fiske, R. S., 1993, Long-term evolution of fluid-rock interactions in magmatic arcs: evidence from the Ritter Range Pendant, Sierra Nevada, California, and numerical modeling: Journal of Petrology, v. 34, p. 23–62.

Helgeson, H. C., Delany, J. M., Nesbitt, H. W., and Bird, D. K., 1978, Summary and critique of the thermodynamic properties of rock-forming minerals: American Journal of Science, v. 278-A, p. 1–229.

Hirschmann, M., 1992, Origin of the transgressive granophyres from the Layered Series of the Skaergaard intrusion, East Greenland: Journal of Volcanology and Geothermal Research, v. 52, p. 185–207.

Hoover, J. D., 1989, The chilled marginal gabbro and other contact rocks of the Skaergaard intrusion: Journal of Petrology, v. 30, p. 441–476.

Ito, E., and Clayton, R. N., 1983, Submarine metamorphism of gabbros from the mid-Cayman Rise: an oxygen isotope study: Geochimica et Cosmochimica Acta, v. 47, p. 535–546.

Jenkins, D. M., 1988, Experimental study of the join tremolite-tschermakite: a reinvestigation: Contributions to Mineralogy and Petrology, v. 99, p. 392–400.

Keenan, J. H., Keyes, F. B., Hill, P. G., and Moore, J. G., 1978, Steam Tables: Thermodynamic Properties of Water Including Vapor, Liquid and Solid Phases: New York, New York, John Wiley and Sons, 156 p.

Kerrick, D. M., Lasaga, A. C., and Raeburn, S. P., 1991, Kinetics of heterogeneous reactions, *in* Kerrick, D. M., editor, Contact Metamorphism: Reviews in Mineralogy, v. 26, p. 583–671.

Kestin, J., 1978, Thermal conductivity of water and steam: Mechanical Engineering, v. 100, p. 1255–1258.

Kridelbaugh, S. J., 1973, The kinetics of the reaction calcite + quartz = wollastonite + carbon dioxide at elevated temperatures and pressures: American Journal of Science, v. 273, p. 757–777.
Kuniyoshi, S., and Liou, J. G., 1976a, Contact metamorphism of the Karmutsen Volcanics, Vancouver Island, British Columbia: Journal of Petrology, v. 17, p. 73–99.
———— 1976b, Burial metamorphism of the Karmutsen volcanic rocks, northeastern Vancouver Island, British Columbia: American Journal of Science, v. 276, p. 1096–1119.
Larsen, L. M., and Watt, W. S., 1985, Episodic volcanism during break-up of the North Atlantic: evidence from the East Greenland plateau basalts: Earth and Planetary Science Letters, v. 73, p. 105–116.
Larsen, L. M., Watt, W. S., and Watt, M., 1989, Geology and petrology of the Lower Tertiary plateau basalts of the Scoresby Sund region, East Greenland: Grønlands Geologiske Undersøgelse, Bulletin, v. 157, 164 p.
Lasaga, A. C., 1986, Metamorphic reaction rate laws and development of isograds: Mineralogical Magazine, v. 50, p. 359–373.
———— 1989, Fluid flow and chemical reaction kinetics in metamorphic systems: a new simple model: Earth and Planetary Science Letters, v. 94, p. 417–424.
Lasaga, A. C., and Rye, D. M., 1993, Fluid flow and chemical reaction kinetics in metamorphic systems: American Journal of Science, v. 293, p. 361–404.
Leake, B. E., 1978, Nomenclature of amphiboles: Canadian Mineralogist, v. 16, p. 501–520.
Lindsley, D. H., 1983, Pyroxene thermometry: American Mineralogist, v. 68, p. 477–493.
Lindsley, D. H., and Anderson, 1983, A two pyroxene thermometer: Journal of Geophysical Research, v. 88 (supplement), p. A887–A906.
Liou, J. G., Kuniyoshi, S., and Ito, K., 1974, Experimental studies of the phase relations between greenschist and amphibolite in a basaltic system: American Journal of Science, v. 274, p. 613–632.
Liou, J. G., Maruyama, S., and Cho, M., 1985, Phase equilibria and mineral parageneses of metabasites in low-grade metamorphism: Mineralogical Magazine, v. 49, p. 321–333.
Loomis, A. A., 1966, Contact metamorphic reactions and processes in the Mt. Tallac roof remnant, Sierra Nevada, California: Journal of Petrology, v. 7, p. 221–245.
Lysak, S. V., 1992, Heat flow variations in continental rifts: Tectonophysics, v. 208, p. 309–323.
Manning, C. E., ms, 1989, Porosity evolution, contact metamorphism, and fluid flow in the host basalts of the Skaergaard magma-hydrothermal system: Ph.D. thesis, Stanford University, Stanford, California, 190 p.
Manning, C. E., and Bird, D. K., 1986, Hydrothermal clinopyroxenes of the Skaergaard intrusion: Contributions to Mineralogy and Petrology, v. 92, p. 437–447.
———— 1990, Fluorian garnets from the host rocks of the Skaergaard intrusion: implications for metamorphic fluid composition: American Mineralogist, v. 75, p. 859–873.
———— 1991, Porosity evolution and fluid flow in the basalts of the Skaergaard magma-hydrothermal system, East Greenland: American Journal of Science, v. 291, p. 201–257.
———— 1993, Porosity, permeability and basalt metamorphism, *in* Day, H., and Schiffman, P., editors, The Transition from Basalt to Metabasalt: Geological Society of America Special Paper, in press.
Maruyama, S., Suzuki, K., and Liou, J. G., 1983, Greenschist-amphibolite transition equilibria at low pressures: Journal of Petrology, v. 24, p. 583–604.
McBirney, A. R., 1989, The Skaergaard layered series: I. structure and average compositions: Journal of Petrology, v. 30, p. 363–397.
McBirney, A. R., and Noyes, R. M., 1979, Crystallization and layering of the Skaergaard intrusion: Journal of Petrology, v. 20, p. 487–564.
McDougall, I., and Harrison, T. M., 1988, Geochronology and thermochronology by the $^{40}Ar/^{39}Ar$ method: New York, Oxford University Press, 212 p.
McKibbon, R., and Tyvand, P. A., 1982, Anisotropic modelling of thermal convection in multilayered porous media: Journal of Fluid Mechanics, v. 118, p. 315–339.
McLean, D., 1965, The science of metamorphism in metals, *in* Pitcher, W. S., and Flinn, G. W., editors, Controls of Metamorphism, New York, New York, John Wiley Sons, p. 103–118.
Meyer, C. A., McClintock, R. B., Silvestri, G. J., and Spencer, R. C., 1979, ASME Steam Tables—Thermodynamic and Transport Properties of Steam: New York, New York, American Society of Mechanical Engineers, 330 p.

Moody, J. B., Meyer, D., and Jenkins, J. E., 1983, Experimental characterization of the greenschist/amphibolite boundary in mafic systems: American Journal of Science, v. 283, p. 48–92.

Murphy, W. M., and Helgeson, H. C., 1989, Thermodynamic and kinetic constraints on reaction rates among minerals and aqueous solutions. IV. Retrieval of rate constants and activation parameters for the hydrolysis of pyroxene, wollastonite, olivine, andalusite, quartz, and nepheline: American Journal of Science, v. 289, p. 17–101.

Myers, J. S., 1978, Skaergaard intrusion, East Greenland: contact metamorphism and deformation on Mellemö: Geological Society of Denmark Bulletin, v. 28, p. 1–4.

Nielsen, T. F. D., 1978, The Tertiary dike swarms of the Kangerdlugssuaq area, East Greenland. An example of magmatic development during continental break-up: Contributions to Mineralogy and Petrology, v. 67, p. 63–78.

Nielsen, T. F. D., Soper, N. J., Brooks, C. K., Faller, A. M., Higgins, A. C., and Matthews, D. W., 1981, The pre-basaltic sediments and the lower basalts at Kangerdlugssuaq, East Greenland: their stratigraphy, lithology, palaeomagnetism and petrology: Meddelser om Gønland, Geoscience, v. 6, 25 p.

Norton, D., 1988, Metasomatism and Permeability: American Journal of Science, v. 288, p. 604–619.

Norton, D., and Knight, R., 1977, Transport phenomena in hydrothermal systems: cooling plutons: American Journal of Science, v. 277, p. 937–981.

Norton, D., and Cathles, L. M., 1979, Thermal aspects of ore deposition, *in* Barnes, H. L., editor, Geochemistry of Hydrothermal Ore Deposits, v. 2: New York, New York John Wiley & Sons, p. 611–631.

Norton, D., and Taylor, H. P., Jr., 1979, Quantitative simulation of the hydrothermal systems of crystallizing magmas on the basis of transport theory and oxygen isotope data: an analysis of the Skaergaard intrusion: Journal of Petrology, v. 20, p. 421–486.

Norton, D., Taylor, H. P., Jr., and Bird, D. K., 1984, The geometry and high temperature brittle deformation of the Skaergaard intrusion: Journal of Geophysical Research, v. 89, p. 10178–10192.

Parks, G. A., 1984, Surface and interfacial free energies of quartz: Journal of Geophysical Research, v. 89, p. 3997–4008.

Parmentier, E. M., and Schedl, A., 1981, Thermal aureoles of igneous intrusions: some possible indications of hydrothermal convective cooling: Journal of Geology, v. 89, p. 1–22.

Porter, D. A., and Easterling, K. E., 1981, Phase transformations in metals and alloys: New York, Van Nostrand Reinhold, 446 p.

Ridley, J., 1985, The effect of reaction enthalpy on the progress of a metamorphic reaction, *in* Thompson, A. B., and Rubie, D. C., editors, Metamorphic Reactions: Kinetics, Textures and Deformation: New York, New York, Springer-Verlag, p. 80–97.

Ridley, J., and Thompson, A. B., 1986, The role of mineral kinetics in the development of metamorphic microtextures, *in* Walther, J. V., and Wood, B. J., editors, Fluid-Rock Interactions During Metamorphism: New York, New York, Springer-Verlag, p. 154–193.

Robinson, P., Spear, F. S., Schumacher, J. C., Laird, J., Klein, C., Evans, B. W., and Doolan, B. L., 1982, Phase relations of metamorphic amphiboles: natural occurrence and theory, *in* Veblen, D. R., and Ribbe, P. H., editors, Amphiboles: Petrology and Experimental Phase Relations: Reviews in Mineralogy, v. 9B, p. 1–227.

Rosing, M. T., and Lesher, C. E., 1992, P-T conditions for metabasalt transformation in the roof pendant of the Miki Fjord Macrodike from the occurrence of spinel, cordierite, and quartz: EOS, v. 73, no. 43 (supplement), p. 640.

Rubie, D. C., and Thompson, A. B., 1985, Kinetics of metamorphic reactions at elevated temperatures and pressures: an appraisal of available experimental data, *in* Thompson, A. B., and Rubie, D. C., editors, Metamorphic Reactions: Kinetics, Textures and Deformation: New York, New York, Springer-Verlag, p. 27–79.

Russ-Nabelek, C., 1989, Isochemical contact metamorphism of mafic schist, Laramie Anorthosite Complex, Wyoming: amphibole compositions and reactions: American Mineralogist, v. 74, p. 530–549.

Schott, J., Berner, R. A., and Sjöberg, E. L., 1981, Mechanism of pyroxene and amphibole weathering—I. Experimental studies of iron-free minerals: Geochimica et Cosmochimica Acta, v. 45, 2123–2135.

Snoke, A. W., Quick, J. E., and Bowman, H. R., 1981, Bear Mountain igneous complex, Klamath Mountains, California: an ultrabasic to silicic calc-alkaline suite: Journal of Petrology, v. 22, p. 501–552.

Soper, N. J., Higgins, A. C., Downie, C., Matthews, D. W., and Brown, P. E., 1976a, Late Cretaceous-Tertiary stratigraphy of the Kangerdlugssuaq area, East Greenland, and the age of the opening of the north-east Atlantic: Journal of the Geological Society of London, v. 132, p. 85–104.

Soper, N. J., Downie, C., Higgins, A. C., and Costa, L. I., 1976b, Biostratigraphic ages of Tertiary basalts on the East Greenland continental margin and their relationship to plate separation in the northeast Atlantic: Earth and Planetary Science Letters, v. 32, p. 149–157.

Spear, F. S., 1981, An experimental study of hornblende stability and compositional variability in amphibolite: American Journal of Science, v. 281, p. 697–735.

Stakes, D. S., and Taylor, H. P., Jr., 1992, The northern Samail ophiolite: an oxygen isotope, microprobe, and field study: Journal of Geophysical Research, v. 97, p. 7043–7080.

Stakes, D. S., Taylor, H. P., Jr., and Fisher, R. L., 1984, Oxygen-isotope and geochemical characterization of hydrothermal alteration in ophiolite complexes and modern oceanic crust, *in* Gass, I. G., Lippard, S. J., and Shelton, A. W., editors, Ophiolites and Oceanic Lithosphere: Geological Society of London Special Publication, v. 14, p. 199–214.

Steefel, C. I., and Van Cappellen, P., 1990, A new kinetic approach to modeling water-rock interaction: the role of nucleation, precursors, and Ostwald ripening: Geochimica et Cosmochimica Acta, v. 54, p. 2657–2677.

Taylor, H. P., Jr., 1977, Water/rock interactions and the origin of H_2O in granitic batholiths: Geological Society of London Journal, v. 133, p. 509–558.

Taylor, H. P., Jr., and Forester, R. W., 1979, An oxygen isotope study of the Skaergaard intrusion and its country rocks: a description of a 55-m.y. old fossil hydrothermal system: Journal of Petrology, v. 20, p. 355–419.

Tracy, R. J., and Frost, B. R., 1991, Phase equilibria and thermobarometry of calcareous, ultramafic and mafic rocks, and iron formations, *in* Kerrick, D. M., editor, Contact Metamorphism: Reviews in Mineralogy, v. 26, p. 207–289.

Turner, F. J., 1981, Metamorphic Petrology: Washington D.C., McGraw-Hill, 254 p.

Wager, L. R., and Brown, G. M., 1967, Layered Igneous Rocks: San Francisco, W. H. Freeman, 588 p.

Wager, L. R., and Deer, W. A., 1939, Geological investigations in East Greenland, Part III. The petrology of the Skaergaard intrusion: Meddelser om Grønland, v. 105, p. 1–352.

Walther, J. V., and Wood, B. J., 1984, Rate and mechanism in prograde metamorphism: Contributions to Mineralogy and Petrology, v. 88, p. 246–259.

———— 1986, Mineral-fluid reaction rates, *in* Walther, J. V., and Wood, B. J., editors, Fluid-Rock Interactions During Metamorphism: New York, New York, Springer-Verlag, p. 194–211.

Watson, J. T. R., Basu, R. S., and Sengers, J. V., 1980, An improved representative equation for thermodynamic viscosity of water substance: Journal Physical Chemistry Reference Data, v. 9, p. 1255–1279.

Wegner, W. W., and Ernst, W. G., 1983, Experimentally determined hydration and dehydration reaction rates in the system MgO-SiO_2-H_2O: American Journal of Science, v. 283-A, p. 151–180.

Wood, B. J., and Walther, J. V., 1983, Rates of hydrothermal reactions: Science, v. 222, p. 554–555.